I-ImaS – Workpackage 3

Deliverable No D.9

"Different approaches to providing intelligence in the sensor/imaging system"

Last Updated: 05-Oct-2009

I-ImaS: Intelligent Imaging Sensors for Industry, Health and Security

FP6-505593-1

Work package No.3 – Image Analysis

Deliverable D.9 – "Different approaches to providing intelligence in the sensor/imaging system"

Contributing Authors:

- CTI: Harris Georgiou, sections: 5.*, 6.*, 8.1.*, 9.*
  mailto: xgeorgio@di.uoa.gr
- SINTEF: Helene Schulerud, sections: Exec.Sum., 3.1.*, 5.1, 6.3.*, 8.2.*, 9.2.1
  mailto: Helene.Schulerud@sintef.no
- UCL: Robert Speller, sections: 4.*, 2.1;
  mailto: rspeller@medphys.ucl.ac.uk
- UoT: Anna Bergamaschi, sections: 1, 7, 9.1
  mailto: bergamaschi@ts.infn.it

Corresponding Author:

Harris Georgiou (UOA/CTI), mailto: xgeorgio@di.uoa.gr

Last Updated: 05-Oct-2009

Contents :

Executive Summary

The objective of the I-ImaS project is to develop a new sensor which adaptively adjusts the exposure settings in order to enhance the image quality or reduce the patient dose. The exposure adjustment is performed by a control system. In this study we have analysed different approaches for such a control system, and one prototype is developed. This is based on the previous work done in identifying suitable information signatures (deliverable D8).

The control system is based on the I-Imas system architecture and specifications as given in deliverable D13 and D14. In this architecture, the tissue is first imaged using a so-called “scout scan”. This initial imaging is done using a constant dose. The data from the scout scan is analyzed automatically in real-time in order to determine the correct exposure for the second scan.

In order to develop a control system the images in the developed database were evaluated by 2 or 3 radiologists.

An analysis of different options for embedding different levels of “intelligence” into the sensor IC, from basic linear adaptive control to sophisticated classifier-based non-linear modules has been performed. This context has been used to select a good framework for developing the control algorithm.

The study includes prototyping of an initial control system algorithm. The algorithm is based on data from a scout scan combined with a pre-established sensor model to predict the correct exposure. The main goal of this algorithm is to avoid underexposure. The algorithm goal was chosen amongst many other candidates, and give consistently good results on the available images. The regulated images from the mammography database were evaluated together with a reference image in a blind test by two experienced radiologists at Ullevål University Hospital in Norway. The reference image was taken with uniform exposure at the highest dose used in the regulated image. All the regulated images were evaluated to have the same or better overall quality than the reference image, however at a lower dose.

The development and the evaluation of the steering algorithm are based on the tissue images in database DB3, which consist of a limited number of tissue samples. Consequently, there is some uncertainty considering the robustness of the algorithm.

There has also been developed a visualization system, which makes the images from the developed sensor appear as though they were captured with a normal, constant-exposure sensor system. This visualization model is based on a model of the sensor.

This study provides an algorithm for both control and later visualization, which has shown initial success in a limited test. The algorithm should be easy to implement on the sensor.

1. Introduction

The peculiar feature of the I-ImaS imaging system is the possibility of obtaining images with an optimized quality in the region including details of high diagnostic interest. This approach allows delivering a high dose of a radiation only to the regions which present a significant radiological interest, thus reducing the overall radiation dose given to the patient.

The main structures to be detected in mammography are the denser regions which might embed masses or calcifications hidden inside the glandular tissue and microcalcification clusters, which are important signatures of the presence of cancer.

An increased exposure is required in order to enhance the visibility of structures embedded in the dense glandular areas and of small calcifications by reducing the noise presence in the image.

The acquisition process is divided in several steps that will be described in detail in this document:

- The data acquired by the detector will be pre-processed in order to be corrected for the detector fixed pattern disuniformities.
- The important statistical quantities calculated in on image sub-areas will be used for recognizing the presence of significant information.
- The exposition settings will be adjusted in order to optimize the delivered dose proportionally to the diagnostic interest of the exposed area.
- Finally the data will be post processed in order to display them. In particular the image will be flat field corrected in order to display coherently regions acquired with different settings, the grayscale will be optimized and possibly some filters will be applied in order to reduce the presence of noise or enhance particular image features.

2. Primary Data

2.1 Mammographic images

A series of mammographic images were taken at UCL to provide the real breast tissue image data base (DB3). These images were taken using a Seimen's Mammomat B and dPix Flashscan 30 flat panel array. The system was set up to simulate clinical conditions except for the use of a secondary radiation grid. The 300 micron focal spot was used with 60 micron Mo filter. The X-ray source target was molybdenum. The tissue was excised full breast slices approximately 1 cm thick. The slices were known to contain both normal and pathological tissue. The tissue was fixed and contained in polythene bags. To simulate a full compressed breast each tissue section was imaged with additional Perspex sheets to make up the full breast. Two tissue slices were made up to an equivalent thickness of 20mm, and two to an equivalent thickness of 40mm. Each tissue section was then imaged over a range of exposure values. An ionization chamber was placed next to the tissue to ensure the Mammomat was correctly exposing the tissue and the readings recorded on REIDS form C. The table below summarizes the conditions that were used.

Tissue slice	Equivalent Breast thickness	kV	mAs values
U01	40mm	28	8, 16,25,40,64,80,100,125
		30	8, 16,25,40,64,80,100,125
		35	8, 16,25,40,64,80
U02	40mm	28	8,16,20,25,32,40,50,64,80,100
		30	8,16,20,32,40,50,64,80,100
		35	8,16,20,25,32,40,50,64
U03	20mm	28	3.2,4,5,6.4,8,10,12.5,16,20,25,32,40,50
		30	3.2,4,5,6.4,8,10,12.5,16,20,25,32,40
		35	3.2,4,5,6.4,8,10,12.5,16,20,25,32
U04	20mm	28	3.2,4,5,6.4,8,10,12.5,16,20,25,32,40,50,64,80
		30	3.2,4,5,6.4,8,10,12.5,16,20,25,32,40,50
		35	3.2,4,5,6.4,8,10,12.5,16,20,25,32,40

Table 2-1: Exposure conditions used during the image acquisition experiments.

Each image was stored as a .tif file.

3. Overview of Image Evaluations

3.1 Evaluation of mammographic images

3.1.1 Image evaluation from Trieste

Two radiologists from Trieste evaluated the tissue image sets U01, U02, U03 and U04. The last two sets were evaluated with and without the possibility of using post processing which consisted of brightness and contrast adjustments. The RIEDS form E was used for the evaluations. The evaluation grades were from -2 to +2. Zero equals adequate, less than zero corresponds to less than adequate and above zero correspond to better than adequate.

Figure 3-1 shows the overall normal and abnormal quality as a function of mAs for each kVp (red= 28, green=30, blue=35kVp) for each of the two evaluators, together the mean and difference between them for image set U03 and U04. The figure shows that there is some deviation between the evaluators, but they have the same trend and level.

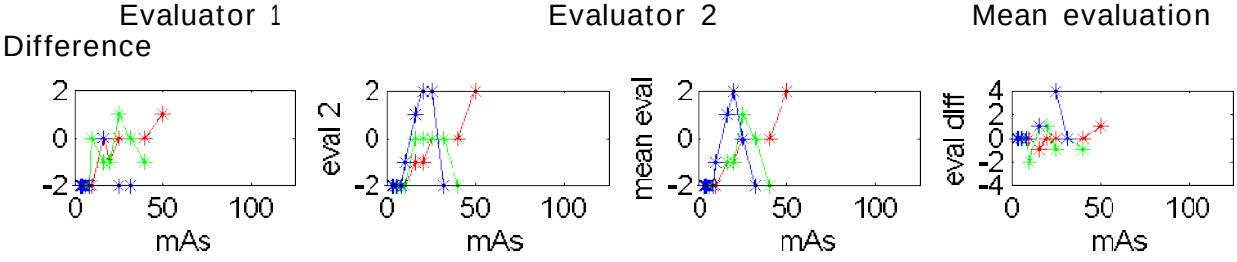

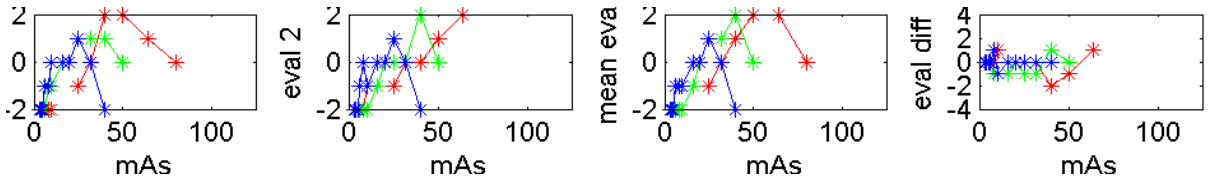

Figure 3-1: Overall normal quality as a function of mAs for each kVp (red= 28, green=30, blue=35kVp) without post processing for image set U03 (upper row) and U04 (lower row).

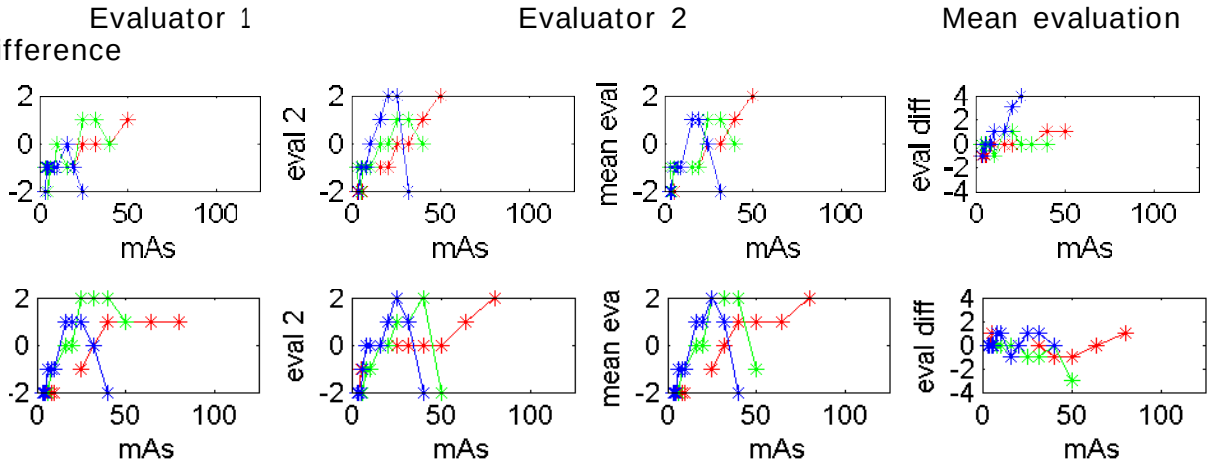

Figure 3-2: Overall abnormal quality as a function of mAs for each kVp (red= 28, green=30, blue=35kVp) without post processing for image set U03 (upper row) and U04 (lower row).

Tables 3-1 and 3-2 show the mean difference between the two evaluators for all the images taken with each kVp. The tables show that the differences between the evaluators with and without post processing do not differ significantly.

kVp	**Mean differance of normal quality**		**Mean differance of abnormal quality**	
	Without postproc.	With Postproc.	Without postproc.	With Postproc.
28	0,2	0,4	0,6	0,3
30	0,6	0,6	0,4	0,4
35	0,7	0,7	1,4	0,4

Table 3-1: Mean difference between evaluators with and without post processing for image set U03.

kVp	**Mean differance of normal quality**		**Mean differance of abnormal quality**	
	Without postproc.	With Postproc.	Without postproc.	With Postproc.
28	0,5	1,0	0,6	0,5
30	0,5	0,6	0,4	0,4
35	0,2	0,5	0,5	0,5

Table 3-2: Mean difference between evaluators with and without post processing for image set U04.

Figures 3-3 and 3-4 show the overall quality evaluations with and without post processing for image set U03. The figures show how most of the images are evaluated as less than adequate when no post processing were allowed. When post processing was used most of the images were evaluated as adequate or better.

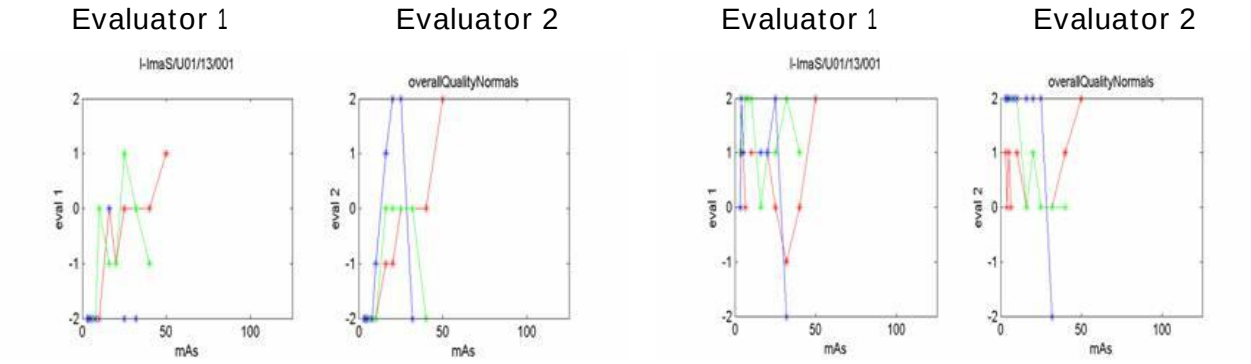

Figure 3-3: Overall normal quality as function of mAs for each kVp (red= 28, green=30, blue=35kVp) without (a,b) and with (c,d) post processing for image set U03.

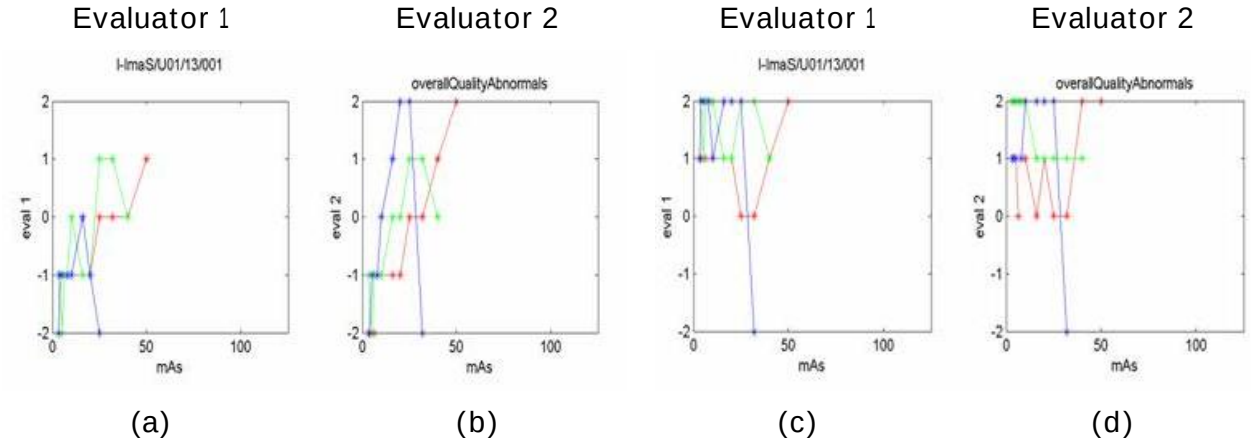

Figure 3-4: Overall abnormal quality as function of mAs for each kVp (red= 28, green=30, blue=35kVp) without (a,b) and with (c,d) post processing for image set U03.

3.1.2 Summary of evaluation from Trieste

The overall normal and abnormal quality evaluation of the images significantly changes with and without post-processing. We view the evaluations with post-processing as most relevant, as we think that it is the image information that should be evaluated, not the image presentation.

For images evaluated with post-processing (U03, U04) almost all the images have overall normal and abnormal quality evaluated as adequate or better. No images with low dose were evaluated as less than adequate, meaning that we did not have images recorded with low quality and low dose. This means that it is

difficult to immediately use these evaluations to choose quality criteria based on image information.

4. Overview of System Design

In total three systems will be evaluated. One for mammography using conventional X-ray sources, one for mammography based around a synchrotron source and one for dental cephlograms. Although basically the same in each case there will be minor differences when the source characteristics are taken into account. Currently most of the design elements have been considered with respect to the conventional mammographic system.

4.1 Conventional mammographic imaging system

The overall system will be based on a dual-in-line scanning system using a molybdenum target X-ray source and X-ray sensitive APS sensors. The dual-in-line detector arrays will scan across the patient whilst the breast is held under compression with the expected scan time to be approximately 3s. The two rows of sensors have different functions. The leading row will form a scout view of the tissue under examination. It will operate at approximately 66% of the total exposure and will be sufficiently high so as to provide information about the suspicious nature of the tissue. The second row of sensors will follow behind with approximately a 1cm gap. The X-ray beam for this row of sensors will be modulated according to a pre-determined model so as to deposit most radiation in regions of high interest and little or no radiation used in regions of low interest. This modulation will be achieved through a series of filters that can be inserted into the beam. The following system components have been identified:

A primary collimator attached to the X-ray source housing that will shape the beam to avoid excessive scattering from other components.

A dual slot collimator before the patient that will divide the beam into a scout beam and an I-ImaS beam.

A filter plate that will accommodate ten wedge filters and actuators suitable for modifying the beam characteristics in a predetermined manner. This plate and its filters could be attached to the dual slot collimator.

A tissue support plate and compression plate. In the prototype system for laboratory evaluation the compression system will not be present and all tissue samples will be pre-compressed.

The detector unit. This will consist of the two rows of sensors and the DAQ board that will communicate with the wedge filters/actuators and acquire the image data from both rows of sensors.

A PC will be used to reconstruct the image data.

4.2 Synchrotron mammographic system

It is intended to use the same components but due to the dimensions of the synchrotron beam it will mean that the scout and I-ImaS views will be acquired separately.

4.3 Cepholometric dental imaging

Dental imaging is carried out with a tungsten target source, aluminum filter and at a kV of between 60 and 65. These characteristics will mean that different wedge filters will be used and a different model to drive the filters will be required. There maybe a need to alter the scintillator type/thickness for the higher energy beam.

5. System Specifications and Constraints

The implementation of a robust and dose-efficient system depends mostly on the “intelligence” of the control mechanism that provides the required adaptiveness to the system. In the case of the I-ImaS sensor IC, the controller design has to be both robust and fast, since the system has to satisfy certain optimality conditions within a very strict time frame.

First, subsection 5.1 presents the specifications and limitations of the current sensor IC. The input parameters, the control variables set and the required output define the general control flow for the on-line module. In subsection 5.2, a formal set of operational profiles are presented in the form of typical description for the final system, as well as the means to define and verify its behavior under nominal conditions.

5.1 System specifications

The I-ImaS system has been proposed as an innovative design for minimizing patient dose while maintaining high levels of quality in the resulting X-ray image. Therefore, it is essential to define the exact criteria that have to be included as optimality conditions by the control mechanism. The general control flow also includes the formal definition of input and output parameters, as well as restrictions and limitations that are inherent to the current sensor IC design.

The final system is specified to have two sensor lines consisting of 16 sensors. Each sensor consists of 512 x 32 pixels resulting in 8192 pixels per row. During scanning the system can regulate the second line by adding more exposure to a given region from 0 to 100% of the possible mAs value using 20% steps. The controlled exposed area corresponds to the sensor size and the sensor size is also used as ROI for analysis and prediction. The time limitation for the algorithm is about 16 ms.

In the first I-Imas prototype system, only the mAs exposure parameter could be changed during the second phase of the scan. The exposure parameters of the scout scan should be sufficient to depicture possible information and is an input parameter to the system. The first scan line of the image can be assumed to be background and is used to calibrate the system.

A characteristic property of the I-ImaS control system is the fact that it is time-critical. Due to the line-scanning procedure and the fact that there is a fixed spatial separation between the first “scout” scan and the second “adaptive” scan, there is only a fixed time interval between the two scans. During this time frame, which in the case of the first I-ImaS prototype is about 16 ms, the control module has to acquire the current input parameters (i.e. exposure settings) and the resulting control set (i.e. extracted textural features) from the first “scout” scan, calculate the current optimality levels (i.e. current image quality versus patient dose) and provide the appropriate feedback (i.e. new exposure settings), in order to guide the

subsequent “adaptive” scan according to the required optimality conditions (i.e. best image quality for minimal patient dose).

The time-critical property of the system affects not only the sophistication and complexity of the control module itself, but also the sophistication and complexity of every other procedure that is included in the same data flow and takes place within the same time window. As a result, every pre-filtering option on the raw data has to be fairly simple and fast, in order to avoid consuming much processing time from the time-critical frame available to the controller module. Similarly, the controller itself has to be able to process the incoming data (exposure), evaluate the current optimality level (output) and calculate the required feedback (adjustment) within the same time frame. Therefore, the decisions related to the time-critical section of the control loop are extremely important for the final system, as they have to closely match the available options of “intelligence” against the capabilities and available resources of the final sensor IC.

The following table summarizes the main specifications for the control module design:

Specification	Parameter	Description
Input Set	{kVp, mAs} or {mGy}	Exposure settings/measurements
Control Set	{textural features}	Internal parameters used by the controller
Output Set	{image quality.vs.dose}	General quantity to be optimized on each run
Constraints	{textural features} {time window} {storage space} {sensor IC speed} {….}	Restrictions imposed by the sensor IC design and the availability of required resources, required by the control module

Table 5-1: General specifications for the control system design

As Table 5-1 shows, there is a choice of using the dose (mGy) instead of the equipment’s exposure settings (kVp, mAs). The dose can be considered as more closely related to the inherent target of the optimization process, which is the minimization of the inflicting dose to the tissue, rather than the current settings used by X-ray source.

The use of just one input parameter, instead of two generally independent input settings, makes the controller design much simpler. Each “scout” scan from the beam provides one set of input raw data, i.e. one set of extracted textural features and one evaluation for the current optimality level. Thus, in order to match the current state of “image quality versus dose” against the current input parameter(s), the kVp and mAs settings would have to be combined into one measurement for the exposure, in this case the inflicting dose. This means that, in practice, the kVp and mAs are not independent if overall exposure level is concerned.

Typically, in modern Automatic Exposure Rate Control (AERC) systems, the dose is measured directly under the projecting plate, using an ionization chamber as a triggering mechanism for cutting off the beam when adequate X-ray exposure has occurred [A01]. The exact values for kVp and mAs are defined by a correlation formula, usually a calculation of the inflicting dose, which is applied according to a

predefined set of Standard Exposure Profiles (SEP) for specific rates of increasing dose, e.g. “standard”, “high contrast”, “pediatric”, etc. Figure 5-1 illustrates similar SEP plans for AERC modes, used in other X-ray applications. Figure 5-2 illustrates the corresponding dose measurements for each SEP option.

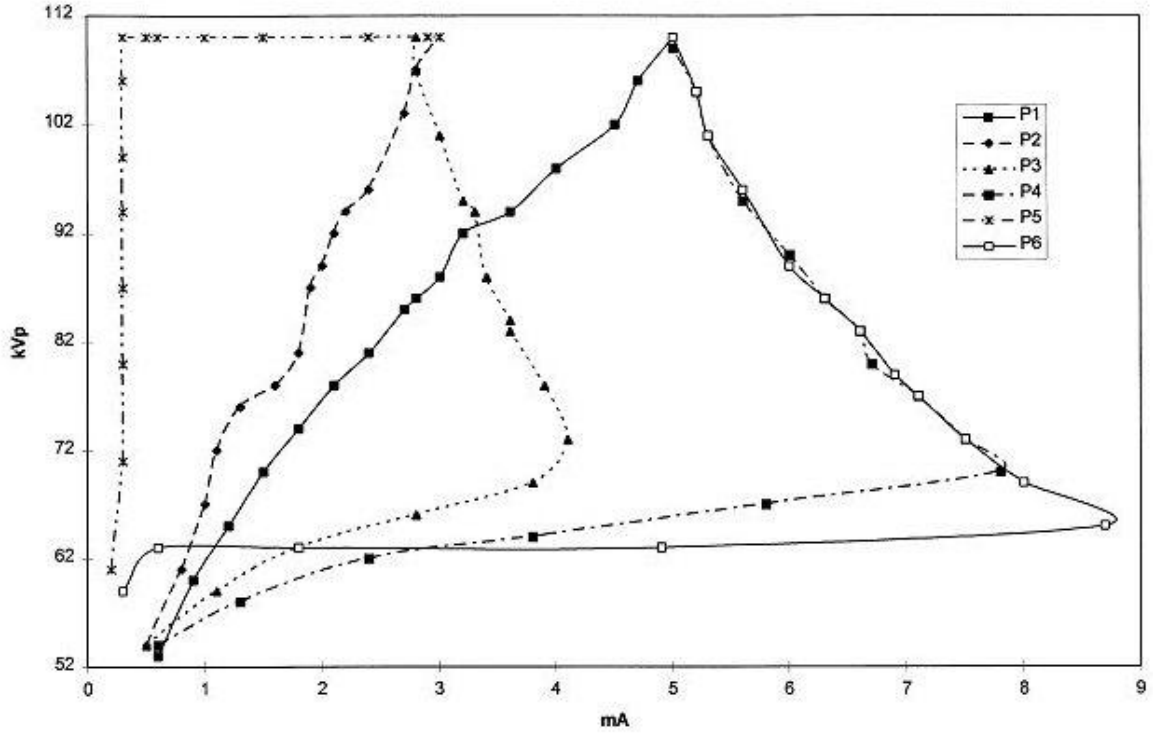

Figure 5-1: SEP profiles: Standard kVp/mAs exposure profiles (AERC) for a modern fluoroscopic unit. P1: standard 5 mA, P2: standard 3 mA, P3: 4 mA high contrast, P4: 8 mA high contrast, P5: “paediatric”, P6: “iodine” [A02].

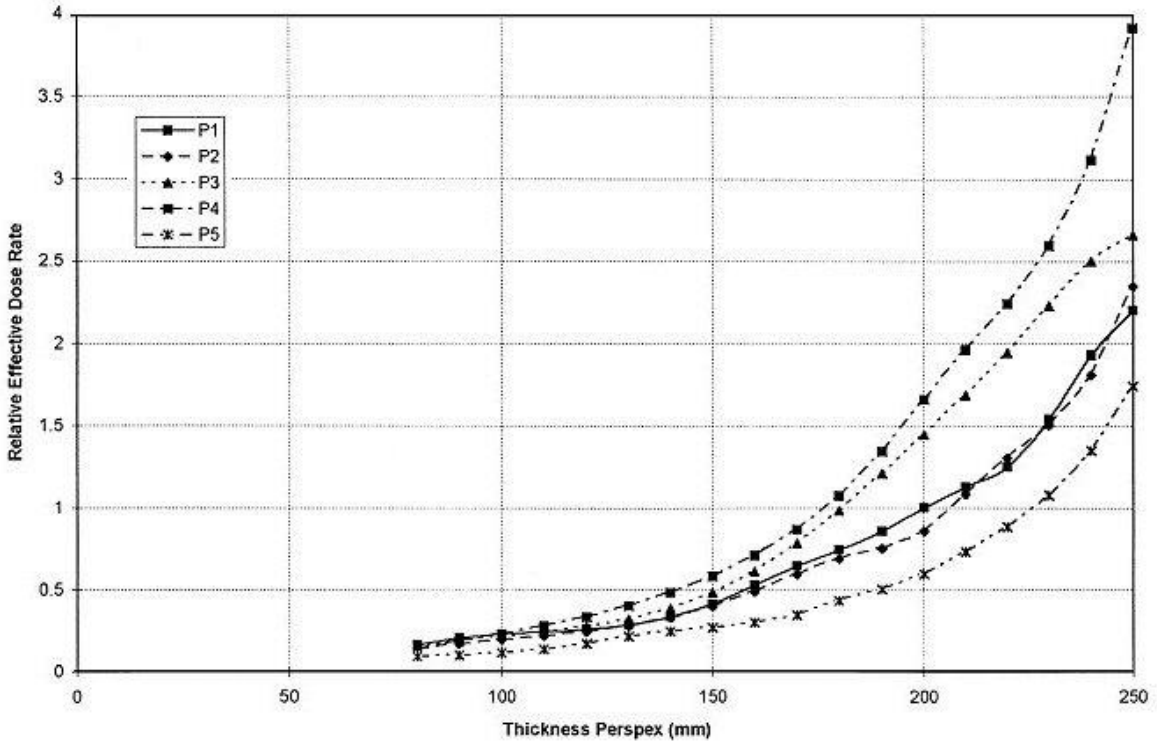

Figure 5-2: SEP doses: Relative patient effective dose (mGy) for a stomach examination at various standard exposure profiles on a conventional X-ray machine [A02].

The option of using SEP plans for the exposure settings is extremely useful for the first I-ImaS prototype for two reasons. First, the current design of the prototype system incorporates a sophisticated mechanism for using wedge filters as an equivalent of adjusting mAs settings, but it does not compensate for adjustments in kVp. This means that the kVp setting has to remain as an "external" parameter, set by the operator before the actual exposure and line-scanning procedure, while the mAs will be the only actual parameter that can be adjusted rapidly during the line-scanning for providing adaptive exposure levels. This means that the adaptive control in the prototype will be responsible for making only mAs adjustments in the exposure, while kVp will remain fixed. This decision policy can be easily incorporated into an appropriate SEP plan similar to the "P6-iodine" curve illustrated in Figure 5.1, where kVp remains constant for the first "flat" section of the curve. The kVp setting can be manually set before the exposure by the operator, according to the thickness or density of the target, similarly to the current clinical practices when using AERC.

The second reason for using SEP plans is related to the use of dose (mGy) as the only input parameter to the control module. Specific SEP curves can be created for specifying optimal inflicting dose according to the requirements of each case, regardless of the system's capability of adjusting only mAs or both mAs and kVp settings on-line. In other words, the control module itself is not bounded to the current capabilities of the sensor IC implementations and it can be employed in any future design of possibly more advanced features. Furthermore, the SEP curve itself can be used as a constraint guideline, prohibiting the use of extreme mAs and/or kVp settings that could result in excessive doses for the tissue.

In the case of the I-ImaS system, the inflicting dose (mGy) can be measured either by using a mechanism similar to the modern AERC systems, e.g. an ionization chamber, or by applying a formal mathematical model for combining the kVp and mAs settings. Normally, the dose can be calculated with the logarithm of a combined parameter, linearly with mAs and exponentially with kVp [A03]:

$$Rx\{mGy\} \quad : \quad f_1(kVp, mAs) = C_{1,1} \cdot \log\left((kVp)^{\alpha} \cdot (mAs)\right) + C_{1,0} \qquad \text{[Eq.5-1]}$$

The degree of the exponent (α) for kVp is normally between 2 and 4, but exact assessment of its value has to be made directly on the specific X-ray system. The first option requires that a dose measurement module has to be embedded in the current sensor IC design, while the second option requires extensive exposure tests on the final geometry and X-ray source of the I-ImaS prototype. In any case, the initial "external" exposure settings kVp and mAs are converted into one combined mGy value that is used as input for the control module.

It should be noted that the efficiency of the final system is closely related to the overall inflicting dose to the patient and not the individual exposure levels for every local section of tissue. This means that, although the exposure level can reach the highest acceptable dose at a specific region of the underlying tissue (e.g. for dense breast or thick tissue areas), the increased exposure level is applied only in these regions and not uniformly throughout the entire breast. Therefore, the percentage of saved dose is closely related to the difference of exposure levels between the first "scout" scan and the second "adaptive" scan of the X-ray beam. The level of the "scout" scan, which is applied throughout the scanning area, should be kept at the minimum possible dose and at the same time provide well-defined textural features for the image processing module. Subsequently, improvement in the feature extraction stage at minimal saturation levels could provide additional savings in the inflicting dose during the second "adaptive" scan, regardless of the efficiency or sophistication of the control module itself.

5.2 Operational profiles

The behavior and operational conditions of the final controller has to be defined in detail, in order to avoid poor results and inconsistencies. Additionally, these formal set of specifications can be used as guidelines for the main task of the design itself. For these reasons, three typical operational profiles can be defined:

- OOP: Optimal Operational Profile
- ORP: Optimal Response Profile
- OCP: Optimal Control Profile

The Optimal Operational Profile (OOP) contains a set of typical constraints for nominal behavior of the system. Essentially, these are the conditions under which the system would operate as expected and would function in an optimal way. The control design for I-ImaS incorporates the extraction and combination of several textural features directly from the resulting image after the first "scout" scan. Therefore, the OOP should take into account and identify the exposure conditions, under which these textural features present the required information content in an acceptable level of quality. Given the set of textural features that will be actually used in the final system, the OOP can use the response curves of each of these features against exposure (dose), in order to identify operational ranges under which these specific features present the best information content quality. Normally, this means that the dose ranges that have to be identified are the ones where these features illustrate consistent and well-defined behavior against dose. For example, a feature function that is "flat" against various levels of dose is not very useful as a control parameter, while another one that is almost linear with non-zero slope could be used instead. If all these features are related directly or indirectly to the current dynamic range of the grayscale, then other global and more general measurements can be used instead. In the case of first-order grayscale statistics, the dynamic grayscale range, i.e. grayscale utilization (%), can

be used as a suggestive measurement for the inherent quality of all the extracted textural features, instead of using their individual response curves. Thus, the OOP could defined the dose ranges under which the grayscale utilization is for example at least 95%, subsequently providing well-defined textural features measurements.

The Optimal Response Profile (ORP) is a formal definition of the optimal behavior of the system itself. In the case of I-ImaS, this is a detailed definition of the property that has to be optimized during the control procedure, i.e. best image quality for minimal dose. The incorporation of two, essentially conflicting, optimality conditions can be realized by combining them into one quantity. Generally, this combination can be implemented using any linear or non-linear functional formulation, but in most cases the simplest way to do this is by converting them into a ratio or into a weighted average. The first option is normally used when the ratio can be directly used as an assessment factor (e.g. a plot of quality versus dose), while the second option is normally used in cases where the resulting quantity is to be used in another subsequent processing stage, like in a control model. Therefore, the second option is the one that is best fit for the design of the control module. The exact form of the weighted average, i.e. the values of the weights applied on “image quality” and on “dose”, can be defined according to the specifications and policy priorities of the system.

Finally, the Optimal Control Profile (OCP) defines the way that the controller is expected to function, i.e. optimize the target quantity while at the same time satisfying certain additional constraints. If the target quantity is the result of a combination of several factors, as suggested by the previous description for the ORP, then the behavioral plan for the controller defines the way that the controller is expected to optimize this quantity while satisfying certain constraints. In the case of I-ImaS, the combined “image quality versus dose” property is expected to be maximized in the second “adaptive” scan of the X-ray beam, provided that the beam’s settings can be adjusted by calculating appropriate feedback for adjustments and provided that these adjustments to the beam result in acceptable dose levels for the current tissue area. Thus, the OCP for the final I-ImaS system could contain a formal definition of the adaptive strategy and calculation of the feedback, using the current input paraneters (kVp/mAs or mGy) and the current control set (textural features values).

6. Controller System Design

The design of an intelligent control module incorporates numerous fields of expertise, including hardware design and implementation, digital filter design, stability study, feedback design and numerical optimization. This section deals with the design issues related mostly to the inherent “logic” of the controller in the form of embedded and/or off-chip software, which is essentially the “heart” of the control module of the system.

Figure 6-1 illustrates the top-level control flow of a typical modern X-ray layout for clinical applications, using AERC as a means of automatic exposure control. The human operator selects a certain “mode” of operation according to the patient’s physical characteristics, including target thickness and tissue type, the saturation in optical density is calculated indirectly using a typical sensor, like an ionization chamber, directly behind the target area, and a simple triggering mechanism uses the sensor output to establish the precise time of X-ray beam cutoff, in order to obtain an X-ray image of expected quality (contrast).

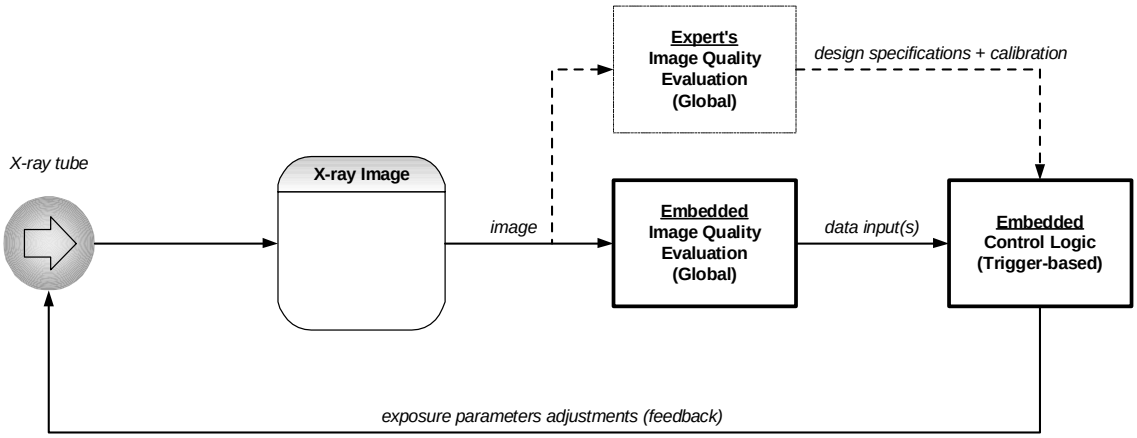

Figure 6-1: AERC model: The external operator sets the initial exposure "mode" using his/hers experience and an automatic triggering mechanism is used as a cutoff switch for the X-ray beam. [A01].

The novel approach of the I-ImaS system comprises from the fact that the image quality evaluation, as well as the adaptive control mechanism, are implemented as embedded modules within the control loop. Therefore, the new system is a closed-loop automatic control model for on-line adaptive X-ray beam driving, using the content of the X-ray image itself as indicators of the resulting quality. Figure 6-2 illustrates the top-level control flow of the closed-loop system, including some details about the intermediate stages of textural feature extraction in the image processing module.

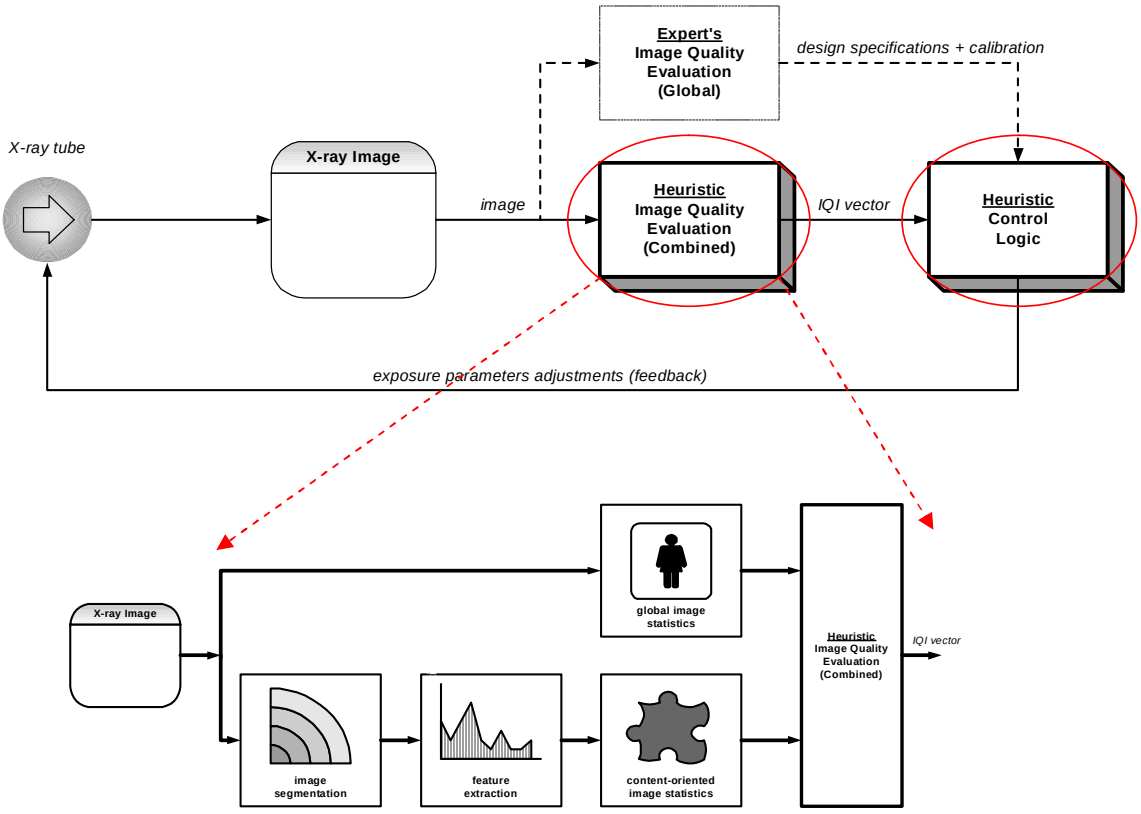

Figure 6-2: I-ImaS model: The external operator is responsible only for monitoring and verification purposes. The I-ImaS system uses automatic image analysis procedures to acquire the current image quality and decides on-line about appropriate adjustments of the X-ray beam during the line-scanning. [A01].

According to the description and constraints of the design task already presented in section 5, the final control flow design can be implemented as follows:

1. The first “scout” beam scans the current tissue area, using fixed kVp and mAs settings
2. The current kVp/mAs are converted into mGy value using a mathematical model
3. The image processing module extracts specific textural features from the resulting image
4. The current dose and textural features values are used to calculate a quality index
5. A generic strategy is used to decide how a new maximal quality index can be obtained
6. The control decision is applied to a formal control model to calculate the current feedback
7. The feedback is adjusted and corrected according to optimality constraints
8. The final feedback is sent to the X-ray source controller before the next “adaptive” scan
9. The X-ray source controller uses feedback from the controller to adjust the beam
10. The second “adapted” beam scans the current tissue area, using adjusted kVp/mAs

All stages from 1 to 3 have been described in detail in previous activity reports and deliverables [A03], while stages 8 to 10 are presented here for purposes of completeness for the overall design.

This section describes thoroughly stages 4 to 7, which constitute the bulk of the control and adaptive mechanism of the I-ImaS system. A generic control model is defined in subsection 6.1 and three levels of sophistications are presented in mathematical form. Subsection 6.2 investigates possible implementations of these sophistication levels, as well as limitations of the current sensor IC. Finally, subsection 6.3 contains a number of suggestive improvements of the current control design, including options for more advanced textural feature extractors, iterative and recursive control loops, as well as neural and fuzzy control modules.

6.1 Generic controller design

The control module in the I-ImaS system can be described in pure mathematical form using state-space description through dynamic equations. The state-space description is generalized method for describing dynamic systems in digital signal processing and automatic control [A04]. In contrast to the traditional description using input-output models, the state-variables embodies a detailed description of the internal properties of the system, including linear or non-linear associations between the input and the output, as well as dynamic transitions of the internal “state” of the system that is not available in a classic “black-box” approach.

This section describes three cascaded approaches for the description of the I-ImaS adaptive control, from the most generic to the most restricted version, using the general mathematical model with gradients (6.1.1), the general model with no gradients (6.2.1) and the linear version with no gradients (6.1.3).

6.1.1 Full state-space description

The state-space description of dynamic systems is a modern, very powerful way of describing the behavior of complex dynamic systems through the introduction of state-variables. The state-variables are a set of internal quantitative attributes of the system, which incorporate and realize the system's behavior under certain conditions. Although an input-output model can describe the characteristic response of a system, stability and consistency can only be evaluated analytically if the internal structure and functionality of the system is described in the same level of detail. Generally, the state-variables can contain a number of properties in the form of internal variables, which are introduced as functional parameters within the dynamic equations of the system. In other words, if the output is dependent to properties other than the input, e.g. the system's internal "state", then these associations can be described through a state-space description.

The general state-space description is incorporated in a system of two dynamic equations, illustrating the functional associations between the input, the output and the internal state-variables:

$$\begin{aligned} \frac{\partial \overrightarrow{x(t)}}{\partial t} &= f\left(\overrightarrow{x(t)}, \overrightarrow{u(t)}, t\right) \\ \overrightarrow{y(t)} &= h\left(\overrightarrow{x(t)}, \overrightarrow{u(t)}, t\right) \end{aligned} \qquad \text{[Eq.6-1a/b]}$$

In Eq.6-1a/b, *u(t)* represents the vector containing all the external inputs to the system, *y(t)* represents the vector containing all the outputs, *x(t)* is the internal state-variables vector and *(t)* is a general spatial or time parameter for non-stationary systems. The first dynamic equation (Eq.6-1a) describes the dependence of the gradient of the state-variables against time- or space-transitions, while the second dynamic equation (Eq.6-1b) describes the association of the output with both input vector and state-variables. Functions *f(.)* and *h(.)* denote general linear or non-linear models for calculating the associated quantities, thus embodying a very powerful and unified way of describing any type of processing, from simple linear transformations to complex neural or fuzzy decision strategies.

When there is the need for a closed-loop system, i.e. the calculation of some feedback in order to apply some on-line adaptive optimization for the resulting output, an additional equation can be added to the system:

$$\overrightarrow{\tilde{u}(t)} = g\left(\overrightarrow{x(t)}, \overrightarrow{u(t)}, t\right) \qquad \text{[Eq.6-1c]}$$

In Eq.6-1c, *g(.)* denotes a generic functional model for calculating the next input vector, not only by the current input and time- or space-parameter, but using the internal state-variables vector as well. This essentially means that *part of the system's internal "state" is used as additional input, in order to "guide" the system towards an intended behavior, i.e. as "feedback"*. Feedback loops are very common in automatic control and they are usually incorporated into a system in order to provide on-line control and/or stabilization [A05].

The implementation of generic non-linear functions in place of *f(.)*, *h(.)* and *g(.)* in the previous dynamic equations makes the analytical description of such systems extremely difficult, if not impossible, in practice. If a system or a control model is exhibits a fairly complex behavioral plan that can not be described in a some simpler way, then the design of the system introduces some heuristic optimization approach, usually named as "training" phase, in order to achieve a pre-defined behavior using some generic modules (e.g. a neural network or an SVM classifier). A simpler and more analytical approach is to approximate the target model with a linear realization and use standard well-formulated methods for investigating its requirements, including stabilization and feedback design. If the system does not permit on-line calculation of gradients due to limited resources or samples, the first dynamic equation (Eq.6-1a) is usually omitted from the model. This later approach is described briefly in the following section.

6.1.2 Restricted state-space description

In the current design of the first I-ImaS prototype, system's specifications suggest that the first "scout" scan over a specific tissue area is the only source of input data for deciding the amount of adjustments in exposure settings before the second "adapted" beam scans the same area. Therefore, only one input "sample" is available for the control mechanism when calculating the feedback for the second phase of each step.

In the case of I-ImaS line-scanning procedure, the main transitional factor is the input itself, i.e. the exposure settings, either kVp/mAs pairs ot mGy single values. Since the system is generally considered stationary, i.e. not varying statistically over time, the on-line calculation of gradients for the state-variables vector requires several instances (calculations) of this vector at different input settings. This means that, in order to calculate the *local* transitions of extracted textural features, *several instances of these features would have to be calculated on the same tissue area, using slightly different exposure parameters*. The current I-ImaS design for sensor IC does not permit varying exposure parameters within the same "scout" scan, therefore it is not possible to apply this mechanism for true gradient calculations in the general case. However, such procedure could be implemented in practice if a generic transition model is available, in the form of "template" transition surface, or if a simple derivative version of can be calculated analytically from the output equation (Eq.6-1b).

If the dynamic system of equations is reduced to a non-differential version as described above, the new "restricted" implementation of the system can be described simply by omitting Eq.6-1a from the mathematical model:

$$\overrightarrow{y(t)} = h\left(\overrightarrow{x(t)}, \overrightarrow{u(t)}, t\right) \qquad \text{[Eq.6-2b]}$$

$$\overrightarrow{\tilde{u}(t)} = g\left(\overrightarrow{x(t)}, \overrightarrow{u(t)}, t\right) \qquad \text{[Eq.6-2c]}$$

Similarly to the description of the generic system of section 6.1.1, Eq.6-2b describes the output of the system and Eq.6-2c describes the feedback.

6.1.3 Restricted linear state-space description

In section 6.1.1, the generic mathematical formulation of the dynamic model was described in detail. However, as mentioned earlier, an analytical form for functionals *f(.)*, *h(.)* and *g(.)* may not be available due to the nature or complexity of the corresponding system modules that implement them. Furthermore, even when such an analytical form is available, the processing time required to calculate them

within the system's main loop may be too expensive or impossible to realize in practice. In the case of I-ImaS, the time-critical nature of the line-scanning procedure makes the choice of these intermediate modules extremely decisive about the success of the system in practice.

A simple and usually adequate implementation solution for time-critical applications is the incorporation of pure linear functions in place of *f(.)*, *h(.)* and *g(.)*. In this case, the dynamic equations for the new system are reduced to linear realizations [A04]:

$$\begin{aligned} \frac{\partial \overrightarrow{x(t)}}{\partial t} &= A \cdot \overrightarrow{x(t)} + B \cdot \overrightarrow{u(t)} \\ \overrightarrow{y(t)} &= C \cdot \overrightarrow{x(t)} + D \cdot \overrightarrow{u(t)} \end{aligned} \qquad \text{[Eq.6-3a/b]}$$

Equation Eq.6-3c describes the most common form of feedback, i.e. the introduction of the state-variables vector in a weighted average along with the current input.

$$\overrightarrow{\tilde{u}(t)} = \overrightarrow{u(t)} + K \cdot \overrightarrow{x(t)} \qquad \text{[Eq.6-3c]}$$

The multiplier *K*, which is a simple constant or a full vector depending on the dimensions of *x(t)*, can be calculated analytically in order to obtain stability and convergence for the final system [A05].

In equations Eq.6-3a/b, the multipliers *A*, *B*, *C*, and *D* are constant vectors or matrices that fully characterize the system's behavior in terms of stability and output calculations. The analytical solution of the system can be formulated as follows:

$$x(t) = \Phi(t - t_0) \cdot x(t_0) + \int_{t_0}^{t} \Phi(t - \tau) \cdot B \cdot u(\tau) \cdot d\tau \qquad \text{[Eq.6-4a]}$$

where $\Phi(t)$ is the solution of the homogeneous equation, i.e.:

$$\frac{\partial x(t)}{\partial t} = A \cdot x(t) \quad \Rightarrow \quad \Phi(t) = e^{A \cdot t} \qquad \text{[Eq.6-4b]}$$

If derivatives of *x(t)* higher than first-order are required, then additional state-variables are introduced in a cascaded derivative scheme, thus the final system includes more state-variables but only first-order derivatives. However, if polynomial realizations of *f(.)*, *h(.)* and *g(.)* are to be used instead of first-order (pure linear) formulations, the analytical solution of such systems becomes much more complex and difficult to evaluate in practice, as in the general case of non-linear models.

The linear state-space description of a control system can be easily converted into a typical input/output equivalent description, using a Laplace transformation of the equations Eq.6-3a/b and calculating the response:

$$H(s) = \frac{Y(s)}{X(s)} = C \cdot (s \cdot I - A)^{-1} \cdot B + D = C \cdot \frac{adj(s \cdot I - A)}{\det(s \cdot I - A)} \cdot B + D \qquad \text{[Eq.6-3d]}$$

6.2 Options for final controller design

The models that were established in the previous sections provide a solid theoretical base for choosing the appropriate model design for the I-ImaS control module. In order to establish an analytical implementation of a custom model, it is essential that decisive choices are clear regarding the nature and structuring of the model's elements.

As mentioned earlier, the time-critical characteristic of the I-ImaS line-scanning procedure and the current design of the sensor IC leads to a minimal implementation for the control module, essentially a pure linear control model similar to the one proposed in section 6.1.3. Furthermore, the introduction of SEP plans for the input (see section 5.1) and a linear function for "image quality versus dose" in the form of weighted average as the output (see section 5.2), lead to a 1-D input/output top-level model for the controller, using the extracted textural features as the internal state-variables vector of the system.

In this section, three levels of sophistication and complexity for the adaptive control are presented in the following sections. In 6.2.1, a very simple approach of single feature usage is presented and analytical results on the system's performance are illustrated accordingly. In 6.2.2, the simple model is extended to include more than one textural feature in the state-variables vector, while in 6.3.3 a complete linear model is introduced, incorporating prior knowledge from expert's evaluation regarding the general performance of the system under certain conditions of exposure.

6.2.1 "Simplistic" linear model

When only one textural feature is used as input for a pure linear control model, a "simplistic" prototype algorithm is produced for the adaptive exposure mechanism of the system. The detailed description of this model and results from its application on the prototype mammographic image database (DB3) are presented in section 6.3.

6.2.2 Extended linear model

Extending the notion and structure of the system that was presented in the previous section, a more complete model can be proposed for using more than one textural feature in the system's state-variables vector. This extension requires a more methodical approach when calculating the mathematical formulation of the final system.

During the first "scout" scan, the image processing module acquires the textural feature values from the primal image of the current tissue area and, subsequently, these feature values are forwarded to an embedded "image quality estimator", along with the current exposure settings. This estimator produces an automatic quality assessment of the current image sample and, given the required minimum level of quality in the resulting final image, the main control module calculates the

necessary adjustments of the exposure parameters, which are required to achieve the specified level of quality (Figure 6-2). Since this procedure is to be completed within one step, i.e. not using iterative optimization techniques, the solution must be calculated analytically using the inverse solutions of the (linear) control model.

The output (target) of the first stage in the control loop is the automatic quality assessment of the current image sample after the first "scout" scan. Since the transition between the current quality index Q_n and the required (optimized) quality index Q_0 includes the transition between the intermediate states of the exposure settings, i.e. the system's input, the mathematical form of this transition can be expressed as:

$$Q_{n+1} = Q_0 = Q_n + \int_{v_n}^{v_{n+1}} \frac{\partial Q_{n,n+1}}{\partial v} \cdot dv \qquad \text{[Eq.6-4]}$$

In Eq.6-4, the integral part in the right side denotes the transition of the quality index as the exposure parameters change. Normally, the calculation of the derivative requires either an analytical formula for the quality index Q_n or at least (*dim*+1) samples around v_n in order to make an arithmetic approximation, where (*dim*) is the number of individual inputs to the system. Even if the input includes only dose (mGy) as suggested in section 5.1, the calculation of the derivative still requires one additional sample for a linear interpolation, which in the case of the current I-ImaS sensor IC will not be available. Therefore, the analytical approach is the only choice, provided that the formula for the quality index Q_n permits rapid calculations of the integral for on-chip implementation.

A simple approach, already suggested by the control model of section 6.2.1, is the definition of the quality index as a simple linear transformation of the available textural feature values:

$$Q_n = y_n = C(\vec{x}_n) \qquad \text{[Eq.6-5a]}$$

In case of fixed linear coefficients, i.e. a weighted average formula, the general form of Eq.6-5a becomes:

$$Q_n = y_n = C_X \cdot \vec{x}_n + C_0 \qquad \text{[Eq.6-5b]}$$

where C_X is the slope and C_0 is the offset of the linear translation.

This type of transformation suggests a pure linear model for the transition plane in the quality index space, which might not be correct in practice. However, if the linear regression of Eq.6-5b can approximate the quality index with an acceptable error, for example by using a Least-Squares-Error criterion for calculating the two linear coefficients, then the calculation of the integral in Eq.6-4 is trivial:

$$Q_{n+1} = Q_0 = Q_n + \left[C_X \cdot \vec{x}_n\right]_{v_n}^{v_{n+1}} \qquad \text{[Eq.6-6]}$$

In order to acquire the final solution for the calculation of the feedback, i.e. the difference between v_n (current settings) and v_{n+1} (next settings), the state-variables

vector x_n has to be formulated analytically against the input v_n as Eq.6-6 suggests. In the general case, this may be very difficult due to non-trivial associations between exposure settings and textural features on the resulting image [A03]. However, if only specific features with linear response curve against exposure level (dose) are selected for the state-variables vector x_n and their analytical form can be approximated in a way similar to the one applied for Eq.6-5a/b, then Eq.6-6 becomes a pure linear functional of parameter v_n and the final solution can be expressed as:

$$\left.\begin{array}{c} x_n^k = \alpha_k \cdot v_n + b_k \\ \vec{x}_n = \sum_k x_n^k = \sum_k (\alpha_k \cdot v_n + b_k) \end{array}\right\} \Rightarrow \Delta Q_{n,n+1} = C_X \cdot \sum_k (\alpha_k) \cdot \Delta v_{n,n+1} \qquad \text{[Eq.6-7a]}$$

$$\text{"}\textit{feedback}\text{"} \quad : \quad \Delta v_{n,n+1} = \frac{1}{C_X \cdot \sum_k (\alpha_k)} \cdot \Delta Q_{n,n+1} = \frac{1}{C_X \cdot \sum_k (\alpha_k)} \cdot (Q_0 - Q_n) \qquad \text{[Eq.6-7b]}$$

As Eq.6-7b suggests, the final calculation of the feedback, i.e. the adjustment in exposure settings, is calculated using a very simple formula that includes the current quality index Q_n and the required quality index Q_0 as a difference. Of course, the linear coefficients should be defined in a way that prohibits division by zero. The simple model presented in section 6.2.1, including only one textural feature x_k as state-variables "vector", can be easily verified as a restricted case of this generic formulation.

The last stage of the embedded implementation in the sensor IC requires the calculation of only one subtraction and one multiplication, provided that the constant part of the formula in Eq.6-7b has been previously calculated and stored in a fast lookup table.

6.2.3 Heuristic extended linear model

In section 6.2.2, the control model included only the state-variables vector as a parameter for calculating the adaptive step towards the intended quality level. In accordance to the general linear equation Eq.6-3b, the full model should include the current input as a factor when calculating the required adjustment for the current exposure settings.

Using the formulation and notion already presented in Eq.6-4 and Eq.6-5a, the full control model can be described as follows:

$$Q_n = y_n = w_C \cdot C(\vec{x}_n) + w_D \cdot D(v_n) \quad , \quad \|w_C\| + \|w_D\| = 1 \qquad \text{[Eq.6-8a]}$$

where $D(v_n)$ is a functional model for translating the current input into contribution to the quality index. The w_C and w_D factors are weighting coefficients for regularizing the amount of contribution to the quality index between the state-variables vector (internal state) and the current input (exposure settings – dose). Thus, *they should be selected in a way that incorporates the priorities policy regarding the quality of the resulting image versus the importance of savings in patient's dose*. Note that the input v_n is not denoted as vector, assuming that dose (mGy) is used instead of kVp/mAs, according to the application of SEP plans already described in section 5.1.

In case of a linear transform for both $C(.)$ and $D(.)$, i.e. a weighted average formula, the general form of Eq.6-8a becomes:

$$Q_n = y_n = w_C \cdot \left(C_X \cdot \vec{x}_n + C_0\right) + w_D \cdot \left(D_V \cdot v_n + D_0\right) \qquad \text{[Eq.6-8b]}$$

where C_X and D_V are the slopes, and C_0 and D_0 are the offsets of the linear regression functions for the two contributing factors.

As already mentioned in the previous section, this type of transformation suggests a pure linear model for the transition plane in the quality index space, which might not be correct in practice. However, if the weighted sum of the two linear regression functions of Eq.6-8b can approximate the quality index with an acceptable error, for example by using a Least-Squares-Error criterion for both, then the calculation of the integral in Eq.6-4 becomes:

$$Q_{n+1} = Q_0 = Q_n + \int_{v_n}^{v_{n+1}} \frac{\partial}{\partial v}\left(w_C \cdot \left(C_X \cdot \vec{x}_n + C_0\right) + w_D \cdot \left(D_V \cdot v_n + D_0\right)\right) \cdot dv \qquad \text{[Eq.6-9]}$$

The integral part in the right side of Eq.6-9 denotes the total contribution of the two factors, i.e. the state-variables vector and the current input, to the quality index, when changing the exposure settings from v_n to v_{n+1} by applying some feedback. The linear form of the weighted average formula inside the integral gives a simple analytical solution for each part:

$$\frac{\partial}{\partial v}\left(w_C \cdot \left(C_X \cdot \vec{x}_n + C_0\right) + w_D \cdot \left(D_V \cdot v_n + D_0\right)\right) = w_C \cdot \frac{\partial}{\partial v}\left(C_X \cdot \vec{x}_n + C_0\right) + w_D \cdot \frac{\partial}{\partial v}\left(D_V \cdot v_n + D_0\right)$$

$$\frac{\partial}{\partial v}\left(C_X \cdot \vec{x}_n + C_0\right) = \frac{\partial C_X}{\partial v} \cdot \vec{x}_n + C_X \cdot \frac{\partial \vec{x}_n}{\partial v} \qquad \text{[Eq.6-10]}$$

$$\frac{\partial}{\partial v}\left(D_V \cdot v_n + D_0\right) = \frac{\partial D_V}{\partial v} \cdot v_n + D_V$$

The top part of Eq.6-10 denotes the analytical calculation of the derivative of the weighted sum inside the integral of Eq.6-9. The derivative of the weighted sum is converted into a weighted sum of the derivatives of the two contributing factors in the right part of Eq.6-9, thus each new derivative is calculated individually in the formulas following the top part of Eq.6-10.

The full solution of Eq.6-10 assumes nothing regarding the parameters C_X and D_V that can generally be non-constant parameters, i.e. varying according to the current exposure settings. Similar generalizations (omitted in Eq.6-10) could also be made for the offset parameters C_0 and D_0 if the activation plan of the control module is implemented as an ensemble of localized linear responses. In the simplest case, where the controller's response function is constituted by only one linear translation, then all the coefficients of the two linear regressions in Eq.6-10 can be regarded as simple constant vectors (for C_X and C_0) or values (for D_V and D_0), and some partial derivatives in Eq.6-10 become zero:

$$\frac{\partial}{\partial v}\left(C_X \cdot \vec{x}_n + C_0\right) = \frac{\partial C_X}{\partial v} \cdot \vec{x}_n + C_X \cdot \frac{\partial \vec{x}_n}{\partial v} \xrightarrow{C_X:const} C_X \cdot \frac{\partial \vec{x}_n}{\partial v}$$

$$\frac{\partial}{\partial v}\left(D_V \cdot v_n + D_0\right) = \frac{\partial D_V}{\partial v} \cdot v_n + D_V \xrightarrow{D_V:const} D_V \qquad \text{[Eq.6-11]}$$

$$\frac{\partial}{\partial v}\left(w_C \cdot \left(C_X \cdot \vec{x}_n + C_0\right) + w_D \cdot \left(D_V \cdot v_n + D_0\right)\right) = w_C \cdot C_X \cdot \frac{\partial \vec{x}_n}{\partial v} + w_D \cdot D_V$$

The derivative of the state-variables vector against the current input parameter in the above Eq.6-11 denotes the transition of the values of the available textural features as the X-ray exposure changes. As already discussed in Eq.6-4, this derivative can be calculated either by using more than one samples around the current "state" and perform an arithmetic approximation of the local slope, or by using some analytical form of the derivative function based on a previous mathematical formulation for the state-variables vector elements.

As in Eq.6-6, this type of transformation suggests a pure linear model for the transition plane in the quality index space, which might not be correct in practice. However, if the linear regression of Eq.6-11 can approximate the quality index with an acceptable error, for example by using a Least-Squares-Error criterion for calculating the linear regression coefficients, then the calculation of the integral in Eq.6-9, using Eq.10 and Eq6-11, becomes trivial:

$$Q_{n+1} = Q_0 = Q_n + w_C \cdot C_X \cdot \left[\vec{x}_n\right]_{v_n}^{v_{n+1}} + w_D \cdot D_V \cdot \left[v\right]_{v_n}^{v_{n+1}} \qquad \text{[Eq.6-12]}$$

Similarly to the model proposed in the previous section, in order to acquire the final solution for the calculation of the feedback, i.e. the difference between v_n (current settings) and v_{n+1} (next settings), the state-variables vector x_n has to be formulated analytically against the input v_n as Eq.6-12 suggests. In the general case, this may be very difficult due to non-trivial associations between exposure settings and textural features on the resulting image. However, if only specific features with linear response curve against exposure level (dose) are selected for the state-variables vector x_n and their analytical form can be approximated in a way similar to the one applied for Eq.6-8a/b, then Eq.6-12 becomes a pure linear functional of parameter v_n and the final solution can be expressed as:

$$\left.\begin{aligned} x_n^k &= \alpha_k \cdot v_n + b_k \\ \vec{x}_n &= \sum_k x_n^k = \sum_k \left(\alpha_k \cdot v_n + b_k\right) \end{aligned}\right\} \Rightarrow \Delta Q_{n,n+1} = w_C \cdot C_X \cdot \sum_k \left(\alpha_k\right) \cdot \Delta v_{n,n+1} + w_D \cdot D_V \cdot \Delta v_{n,n+1} \quad \text{[Eq.6-13a]}$$

$$\text{"}feedback\text{"} : \quad \Delta v_{n,n+1} = \frac{1}{w_C \cdot C_X \cdot \sum_k \left(\alpha_k\right) + w_D \cdot D_V} \cdot \Delta Q_{n,n+1} = \frac{1}{w_C \cdot C_X \cdot \sum_k \left(\alpha_k\right) + w_D \cdot D_V} \cdot \left(Q_0 - Q_n\right) \qquad \text{[Eq.6-13b]}$$

As Eq.6-13b suggests, the final calculation of the feedback, i.e. the adjustment in exposure settings, is calculated using a very simple formula that includes the current quality index Q_n and the required quality index Q_0 as a difference. Of

course, the linear coefficients should be defined in a way that prohibits division by zero. The simple model presented in section 6.2.1, including only one textural feature x_k as state-variables "vector", as well as its first extension, presented in section 6.2.2, can be easily verified as restricted cases of this generic formulation.

The physical meaning and importance of introducing current input, as a second contributing factor when calculating the feedback, is vital. *The second factor of the right part of Eq.6-8a can be explained as the application of "a-priori" knowledge about the transition plane in the quality index space, as the exposure settings change*. This means that if one or more human experts can evaluate the X-ray machine's performance under normal conditions, using a typical target (phantom or real tissue) and applying the complete envelope of the exposure settings, then their average quality assessment on the resulting images can be formulated into a "template" model. This template can be used as additional feed to the system, in accordance to the discussion in section 6.1.2 regarding methods of designing the feedback (Eq6-2c). For I-ImaS, the evaluation sheets, already available by mammography and dental experts, can be exploited in a way that *the control module uses the "template" model as a global quantitative guideline*, which is combined with the extracted textural features of the current tissue area, in order to estimate the optimal adjustment step for the exposure parameters. In practice, this means that if a linear regression model can be calculated for the experts' average quality index against exposure (dose), then *this model can be embedded directly into the controller's logic as additional "intelligence"*, according to the solution presented in Eq.6-13b.

The last stage of the embedded implementation in the sensor IC requires the calculation of only one subtraction and one multiplication, provided that the constant part of the formula in Eq.6-13b has been previously calculated and stored in a fast lookup table.

6.3 Implementation and results of the "simplistic" linear model

The main objective of the simplistic linear steering algorithm is to control the exposure parameters adaptively over the image in order to optimize the image quality compared to the dose.

We have considered several alternative strategies for steering algorithms. These considerations have been made based on our experience with different image features and by inspecting available images with abnormalities.

The following bullets detail some of the choices we have considered, and a brief evaluation of each possibility.

(a) Ensure sufficient grey tone variation within a region of suitable size

This idea was based on how our eye works. A human eye can typically distinguish 200-300 grey levels. Thus, an algorithm which ensures such a variation within any suitable region would ensure that sufficient information was present in the image. Typically this could be implemented by for instance using the standard deviation within local regions, and ensuring that this measure was above a certain level.

Used alone, this feature has several problems. First, it would dramatically overexpose regions that actually were homogenous, as it would strive to achieve an intra-region variation that actually is not present. Secondly, if a region contains both dense and non-dense tissue, the region will typically be underexposed. This happens as the grey tone histogram would contain two peaks, and it is difficult to reliably measure the individual peak widths in multi-peak intermixed greyscale histograms. Figure 6-3 shows a tissue sample (U01) from DB3 together with the standard deviation values measured within each image region. The figure shows

how the standard deviation corresponds to high gradient transition zones like background- foreground and from non-dense tissue to dense masses.

(b) Use of skewness for detecting micro-calcifications

Previous work suggested that local distribution skewness may indicate micro-calcifications (see deliverable D8). However, when using the sensor size as region of interest no correlation between the distribution skewness and areas with micro-calcification was found in images from DB3, see Figure 6-5. Secondly, micro-calcifications are only one of many abnormal features and therefore additional features would be needed.

(c) Use the mean level to control exposure

Another choice is to let the exposure level be proportional to the mean level of any individual region in the scout scan. We are thus basically making the exposure level proportional to the average density of any region. Tumours may be denser than other tissue, and will thus get more exposure. However, the mean level has the some of the same problems as standard deviation with regions containing both dense and non-dense tissue. In such regions, an incorrect estimate can be made resulting in over- or underexposure.

(d) Use a robust estimate of maximum and minimum to control exposure.

This is equivalent to use the scout scan to predict the exposure parameters necessary to avoid under- and overexposure. This strategy has a number of advantages. It will adjust the exposure to make it proportional with the density of the underlying tissue. Thus, it shares the property of the mean by increasing the exposure in dense masses. However, unlike the mean, it will perform well also within regions that contain both dense and non-dense tissue, like blood vessels and possibly also regions containing micro-calcifications.

In order to get a robust estimate of the maximum and minimum value within a region we have chosen to use the 5 and 95 percentile of the greyscale histogram within each region of interest. Figure 6-3 shows the tissue image U01 from database DB3 with abnormal features marked by radiologists (left).The radiologists recognized 1) as a mass element, 2) as an asymmetric density element and some of the radiologists recognized micro-calcifications in the region 3).

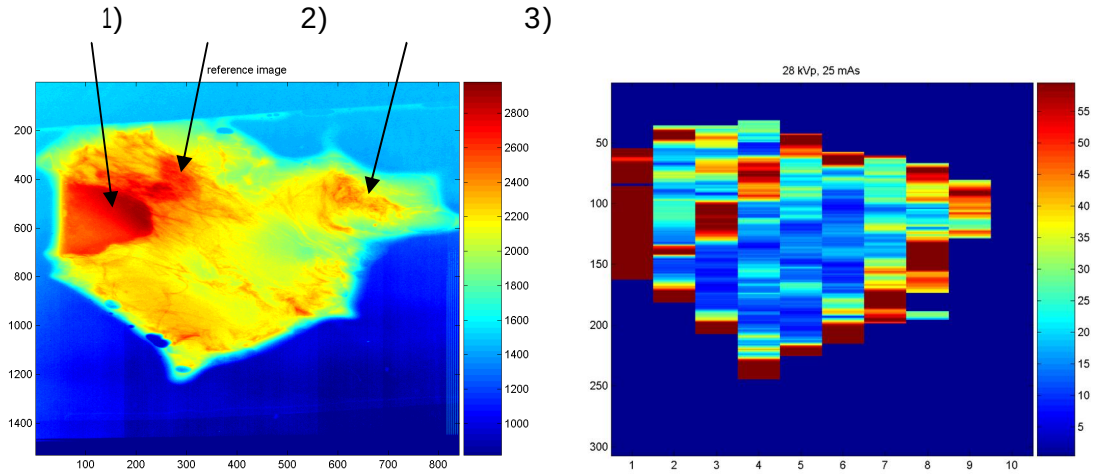

Figure 6-3: Tissue image U01 from database DB3 with abnormal features marked by radiologists (left). The standard deviation of the same tissue image (right) using sensor sized regions.

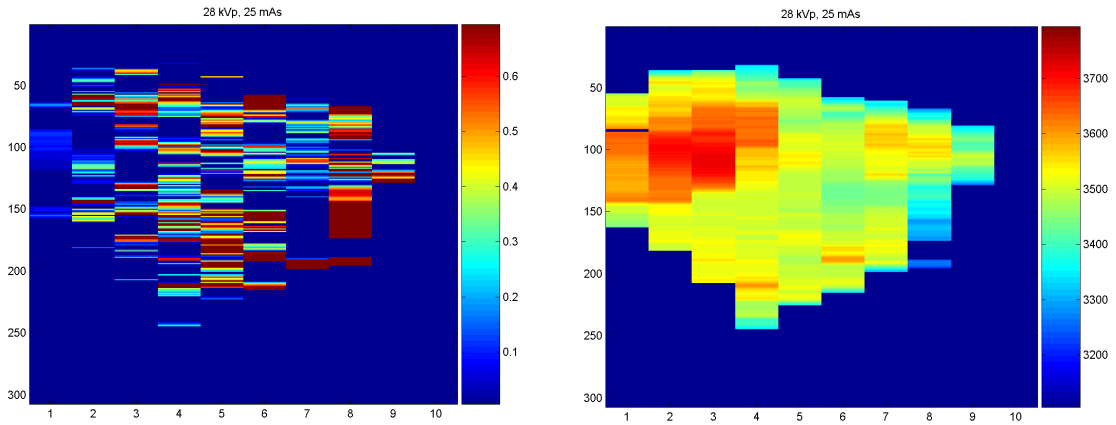

Figure 6-4: The region distribution skewness of tissue image U01 (left) and 95 percentile (right).

We have chosen to implement the latter strategy with an additional layer which makes a distinction between foreground and background. In the foreground/object the mentioned min/max algorithm is used, while in the background a fixed exposure is used. The strategy may seem overly simple, but behaves well in actual experiments, and seems to detect abnormal tissue as well as adjust exposure accordingly. This detection occurs as abnormal tissue tends to include some dense tissue, which is detected and results in increased exposure.

6.3.1 Prediction of correct mAs value

Our algorithm strategy is to use the scout scan to avoid under- and overexposure in the final image. In order to do this, we need to answer the following questions:

- What – exactly – is meant by over- and underexposure?
- Having to choose between over- and underexposure, what will we choose?
- How can we use the information from the scout scan to control the second scan?

(a) Defining under- and overexposure

We have chosen to define overexposure as an exposure setting that will make the sensor saturate. In a real world setting, we do not believe that this will be a problem, so we will not elaborate further on the concept. Moreover, if the scout scan has already overexposed the region, the only possible feedback to the second scan is no additional exposure.

Underexposure is more challenging to define, but is also the most interesting concept. We are interested in using the lowest possible exposure that will avoid underexposure. More theoretical studies have used a variation over the signal-to-noise ratio, as the contrast-to-noise ratio posed by Huda et al [H01].This definition is however not immediately applicable in our case, as this moves the question to defining what “signal” means – as seen by a radiologist.

The test image database does not contain images with sufficient span in quality as evaluated by a radiologist. This has made it difficult to make any data-founded interpretation of “signal”. This lack of data has made us choose a simple definition of underexposure. We have chosen to define underexposure as the mAs value that makes the grey level corresponding to the 95 percentile of the data contained in the second scan larger than a predefined threshold. The exact threshold needs to

be determined empirically by asking radiologists to evaluate images with a suitable range of exposure from the actual sensor.

(b) Choosing between under- and overexposure

This situation will only occur in regions that contain two different materials of significantly different density. We believe that this will be a very rare case in real world scenarios, given a suitable analogue gain setting.

However, in the mammography case, the dense tissues are typically the most interesting, as they typically can be tumours. We have therefore chosen in such cases to overexpose the image.

A consequence of this decision is that the robust regional minimum value is ignored, as we choose to make no efforts to avoid overexposure.

(c) Using data from the scout scan to predict exposure

The algorithm should use the scout scan to predict exposure. In order to do this, the algorithm needs a model of how the sensor behaves for varying mAs values and optical densities.

More precisely, it will need to use the observed grey values in the scout scan to predict the correct exposure. A sensor intensity response model for different mAs and kVp settings has been developed as part of the visualisation module. This model M allows us, given that we have observed grey level G with mAs setting D, to predict what the grey level G' would be if the same object had been observed with mAs setting D'. In mathematical terms:

$$G' = M(G, D, D') \qquad \text{[Eq.6-14]}$$

The model developed in the visualisation module is linear. In this setting, let M(.) be the sensor model, G0 be the grey levels observed in the scout scan, and D0 be the dose for the scout scan. Let further G1 be the grey levels actually observed in the second scan using the dose D1, and G1' be the predicted grey levels observed in the second scan. G1 is unknown at the time of the scout scan, while D1 is to be predicted.

Let P95(.) be a function calculating the 95 percentile of any grey levels observed.

As discussed in sections above, correct exposure is equivalent to ensuring P95(G1) < T where T has been determined empirically. As the model developed in the visualisation module is linear it is reasonable to assume that

$$P95(G') = M(P95(G), D, D') \qquad \text{[Eq.6-15]}$$

as the ordering of the grey levels are maintained in a linear transform. Sensor noise may affect this ordering, but as Figure shows, the assumption seems reasonable.

Given this assumption, we are thus interested in finding a D1 such that

$$P(G1') = M(P95(G0), D0, D1) < T. \qquad \text{[Eq.6-16]}$$

We can only choose between five different D1 values. Determining the correct D1 value is thus done through evaluating all possible D1 values, and selecting the minimum D1 dosage that still fulfils the equation above. This selection needs to be

made beforehand for all possible values of P95(G0). However, this will be a one-time calibration job. This calibration is detailed in section 9.2.1.

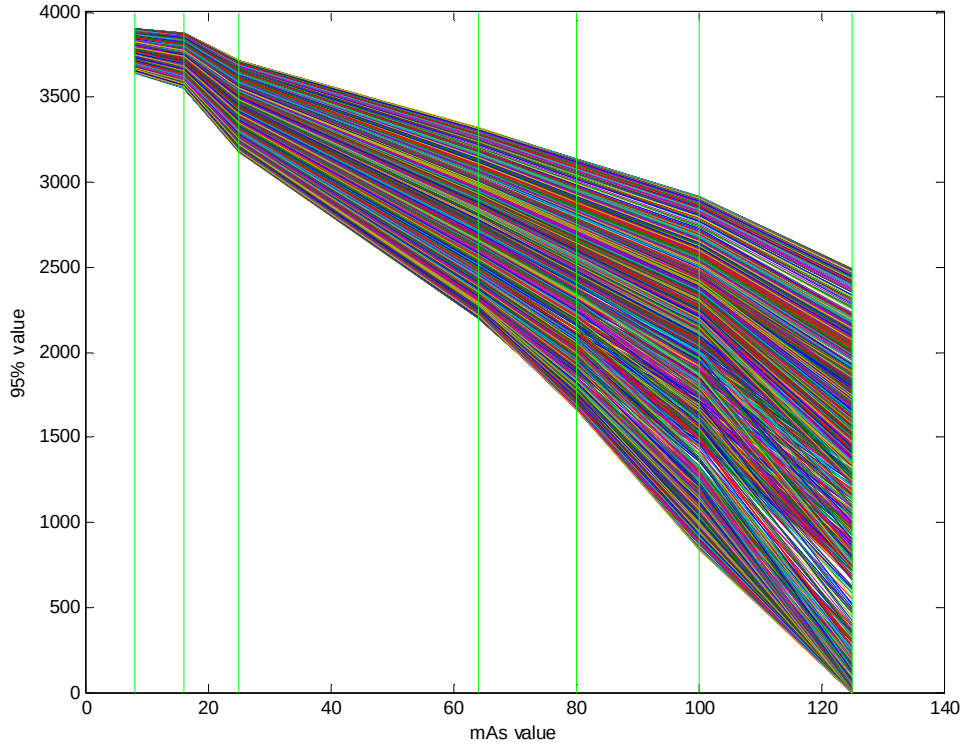

Figure 6-5: Value of 95 percentile as function of mAs for U01 image, 28 kVp. Individual lines show measured 95 percentile values for individual regions in the image. Vertical green lines indicate the mAs values found. The noisy region in the bottom of the original image has been excluded.

6.3.2 Actual linear steering algorithm

This section details the actual steering algorithm. First, an optional pre-processing step is run. The goal of this step is to differentiate between foreground/object and background regions.

*IF (σ(ROI) > BackgroundParameter *σ _Background) AND (μ (ROI) > μ (Background) +BackgroundParameter* σ (Background))*

THEN Foreground state =1;

ELSE (continue Background state)

ENDIF

In the background state, the lowest exposure setting available is used for the second scan.

In the foreground state, the 95 percentile is used to control exposure. Let P95(G0) represent the 95 percentile value of the scout scan data in a region. Let further ADD-p represent a function indicating that an exposure should be used

equivalent to p percent of the maximum second scan exposure. TGi are thresholds established by the routine discussed in section 9.2.1.

IF (Foreground)
IF P95(G0) < TG1 THEN ADD-0
ELSEIF P95(G0) < TG2 THEN ADD-20
ELSEIF P95(G0) < TG4 THEN ADD-40
ELSEIF P95(G0) < TG4 THEN ADD-60
ELSEIF P95(G0) < TG5 THEN ADD-80
ELSE ADD-100;
ENDIF

If the first scan line is not imaging the background the one state model should be used, meaning that there is no differencing between background and foreground and the 95 percentile steering parameter is used all over the image.

6.3.3 Results using the simplistic linear steering model

The algorithm has been tested on both mammography and cephalograms images. The images were regulated using the linear steering algorithm applying 6 possible exposure levels for regulating the second scan. The control-parameter vector (Ti) was estimated using the images of each tissue from database DB3 and the cephalograms images from DB4.

The regulated images of each breast tissue and the cephalogram phantom are shown in Figures 6-6 to 6-15. The figures also show the mAs images representing the mAs value applied in the different image regions. In the blue areas no addition al exposure is added. The regulated images corrected with the visualization algorithm are also shown together with the reference image. The reference image corresponds to the image taken with highest exposure parameters uniformly over the image.

Figure 6-6 shows how the dense areas have received high additional exposure while background and non-dense tissue have received zero or low additional exposure. For tissue U01 shown in Figure 6-6 the dense areas with increased exposure correspond well with the mass element, the asymmetric density element and the micro-calcification area recognized by the radiologists.

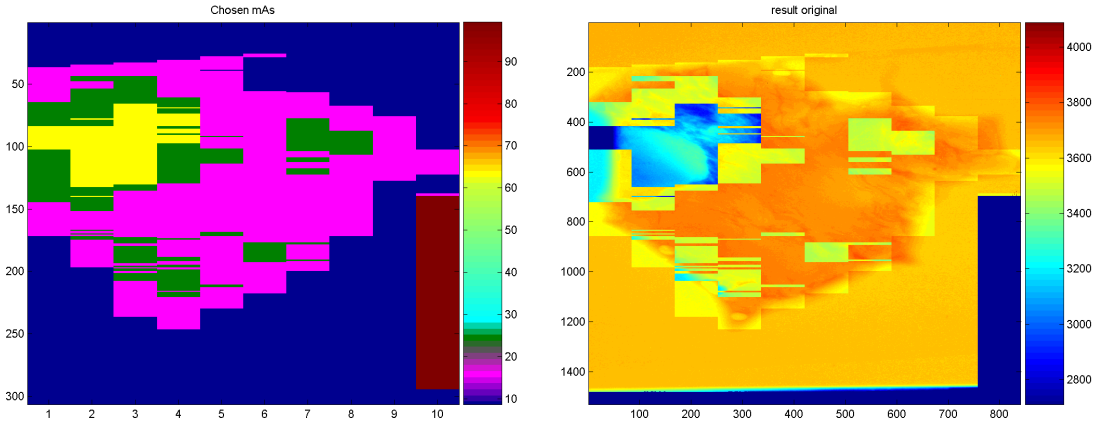

Figure 6-6: Tissue U01 mAs image (left) and regulated image (right).

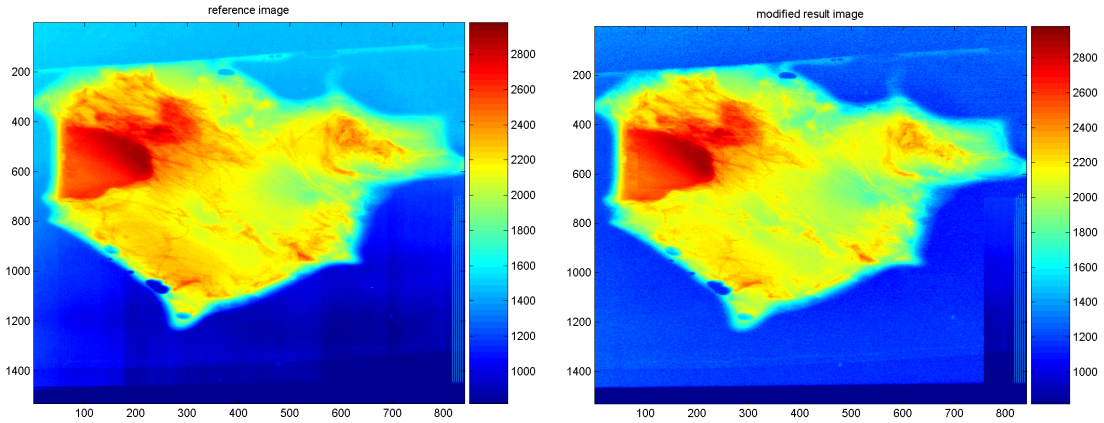

Figure 6-7: Tissue U01 reference image (left) and visual corrected regulated image (right).

For tissue sample U02 no abnormal elements were found by the radiologists. Figure 6-8 shows the regulated image and the corresponding mAs image. Additional exposure is given in the dense areas as expected, even though no abnormal features are present.

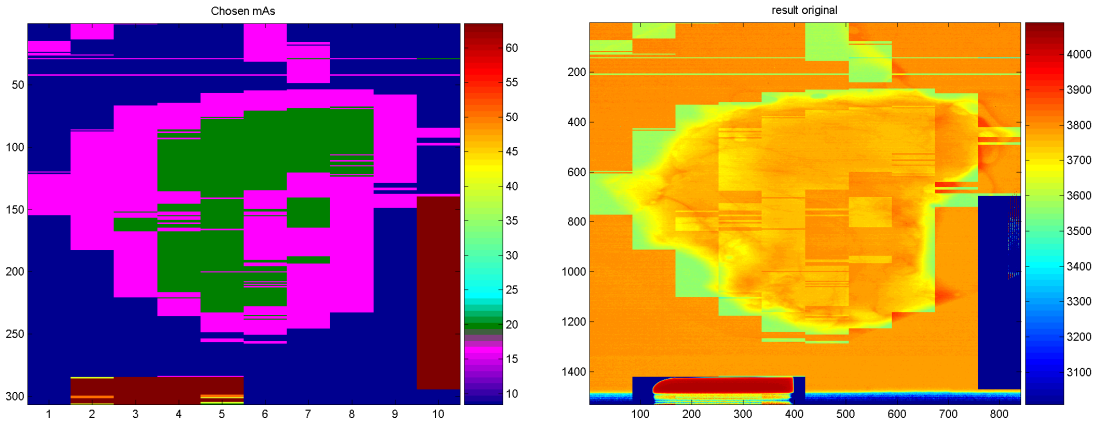

Figure 6-8: Tissue U02 mAs image (left) and regulated image (right).

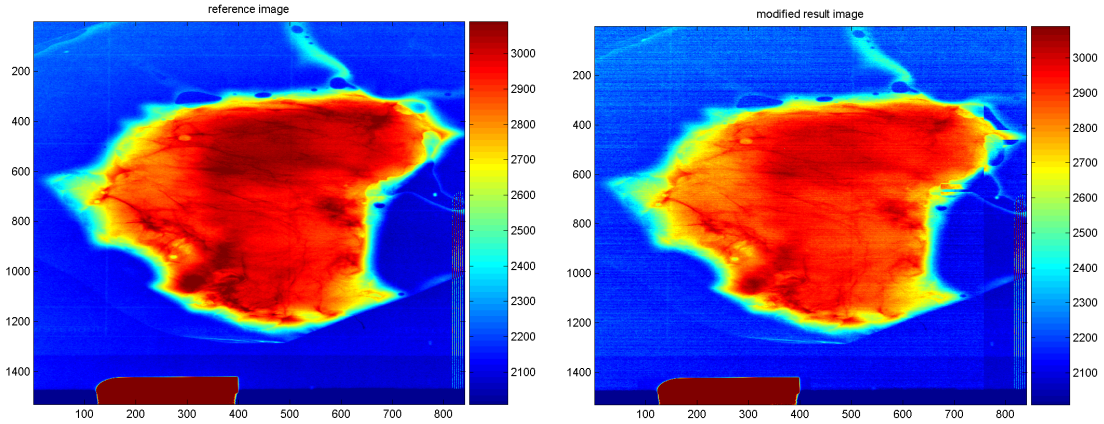

Figure 6-9: Tissue U02 reference image (left) and visual corrected regulated image (right).

For tissue sample U03 an asymmetric density element was recognized by the radiologists. This area has high intensity values, and received additional exposure. However, some other dense tissue with the highest intensity values received the highest additional exposure, see Figures 6-10 and 6-11.

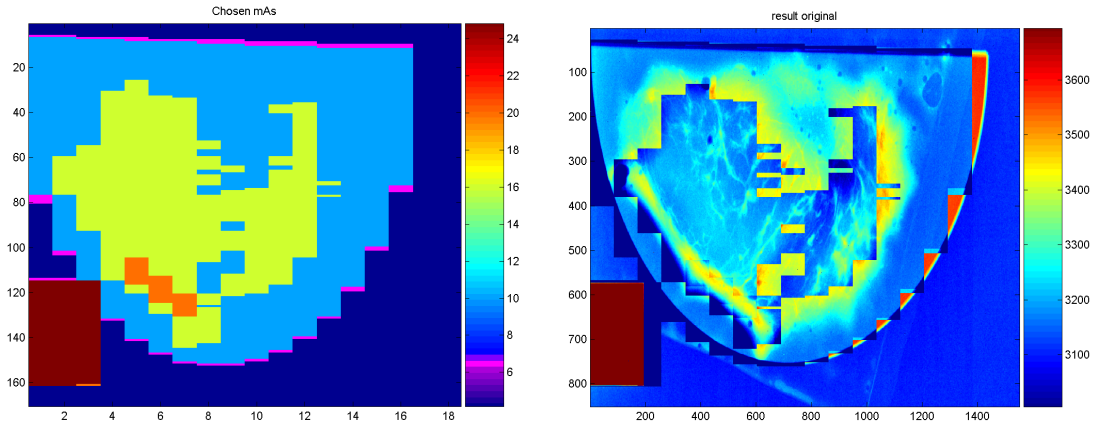

Figure 6-10: Tissue U03 mAs image (left) and regulated image (right).

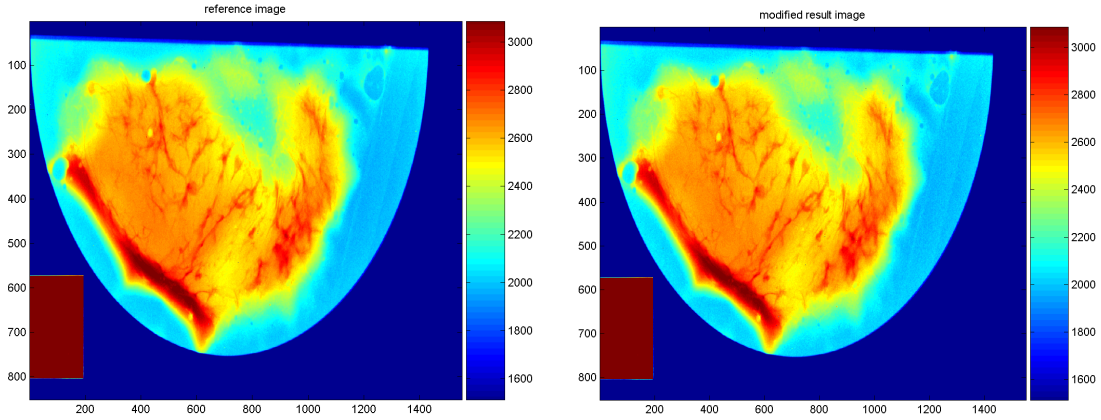

Figure 6-11: Tissue U03 reference image (left) and visual corrected regulated image (right).

In Figures 6-12 and 6-13 the regulation of tissue sample U04 is shown. For this sample a mass element and an asymmetric density element were recognized by the radiologists. In these areas the regulated image has received the highest additional exposure.

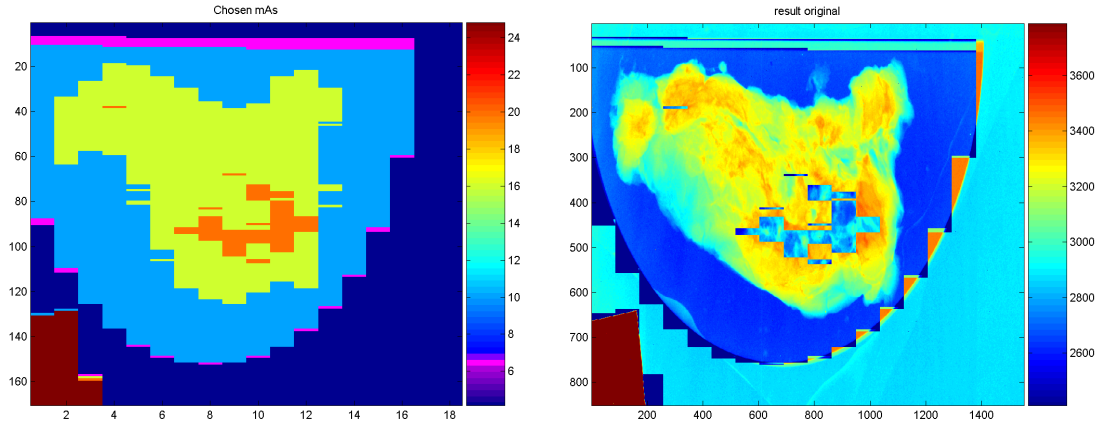

Figure 6-12: Tissue U04 mAs image (left) and regulated image (right).

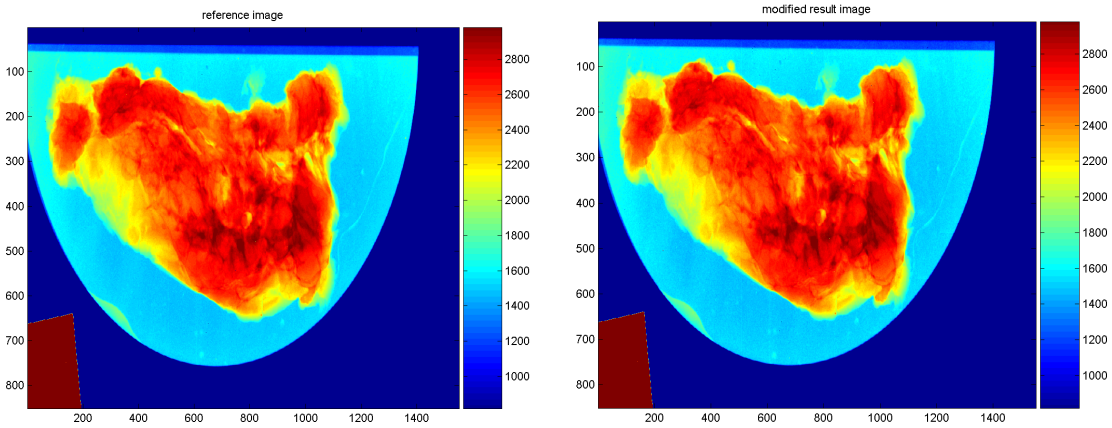

Figure 6-13: Tissue U04 reference image (left) and visual corrected regulated image (right).

The regulated mammography images were evaluated by two experienced radiologists at Ullevål University hospital. The RIEDS form E was used and the evaluation scores used were: -1 as not adequate, 0 as adequate, +1 as good and +2 as excellent. The radiologist evaluated the regulated images and the reference images without knowing anything about the images. One of the radiologists evaluated all the regulated and the reference image equally, while the other radiologist evaluated the regulated image sometimes as good compared to the reference image as adequate. All the images, both the regulated and the reference images were evaluated having an overall quality as adequate or good.

The surface dose (mGy) was measured for all images acquired. The surface dose of the reference image and the regulated image are shown in Table 6-1.

The development and the evaluation of the steering algorithm are based mainly on the tissue images in database DB3 which consist of a limited number of tissue samples. Consequently, there is some uncertainty considering the robustness of the algorithm.

Tissue	Dose regulated image	Dose reference image	Dose savings
	(mGy)	(mGy)	(%)
U01	2,3	7,7	70
U02	1,8	5,0	64
U03	38,8	65,3	41
U04	53,3	79,6	33

Table 6-1: Surface dose of the reference image compared to the regulated image and the dose savings of the regulated images.

In Figures 6-14 and 6-15 the regulation of the Cephalograms is shown. The steering algorithm works as expected and the visualized regulated image seems very similar to the reference image, however captured at a lower dose.

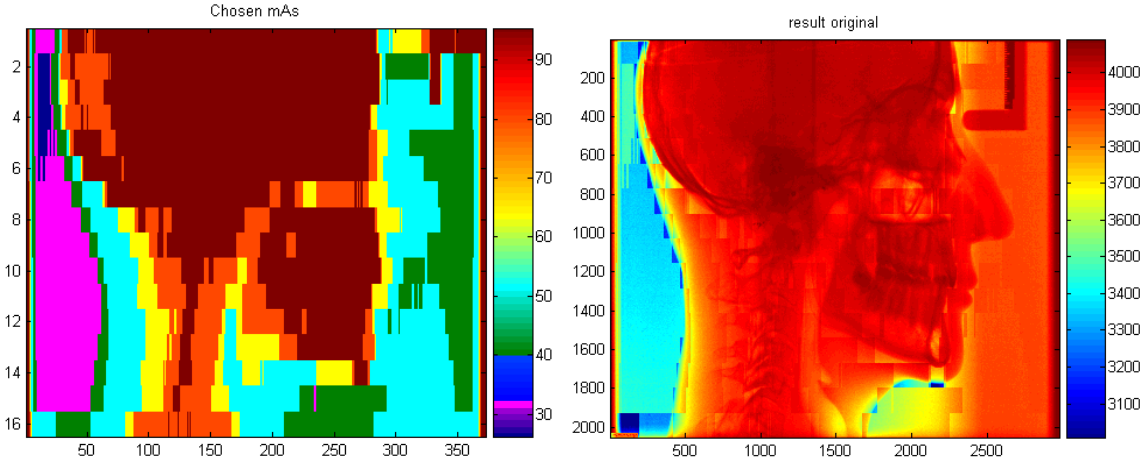

Figure 6-14: Cephalograms mAs image (left) and regulated image (right).

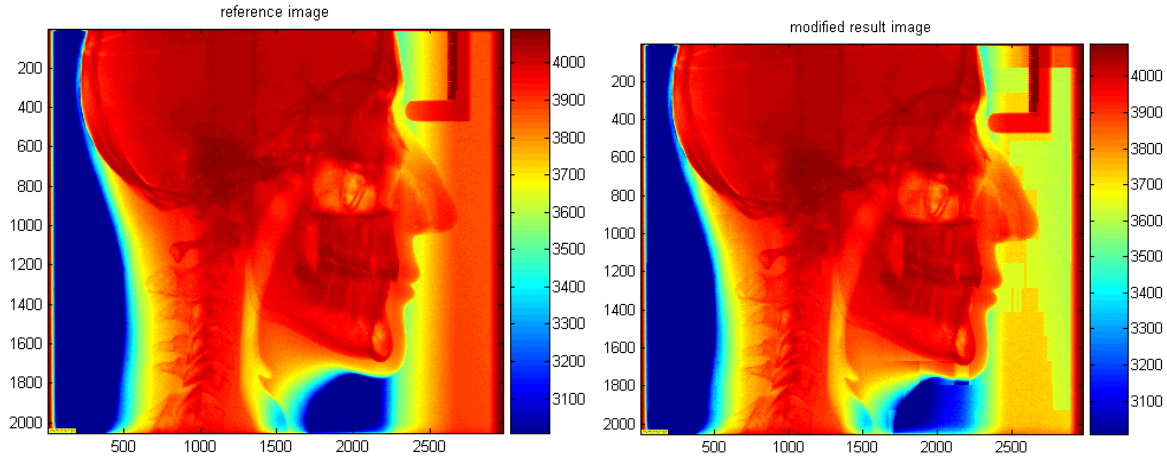

Figure 6-15: Cephalograms reference image (left) and visual corrected regulated image (right).

6.4 Future prospects

In this section, additional options for improving the efficiency and level of sophistication for the sensor IC intelligence are presented. Short descriptions are provided for possible use and advantages of improved textural feature functions (6.3.1), on-chip image restoration (6.3.2), iterative quality optimization and feedback (6.3.3), causal models for recursive filtering (6.3.4), and advanced non-linear control modules (6.3.5). In the scope of I-ImaS, some of these options are related to medium-term improvements of the current specifications and design of the system, while others may be options for future or alternative designs of the sensor IC functionality.

6.4.1 Advanced feature extractors – 2nd order statistics

The image processing stage of the control loop deals with the extraction of specific textural features of the underlying image during the first “scout” scanning phase. Due to the limited dose and the fixed exposure settings during this phase, this primal image is expected to exhibit information content of degraded quality, in terms of both contrast and (possibly) noise. Furthermore, the time-critical characteristic of the line-scanning procedure and the embedded implementation prohibits the application of complex, time-consuming functions within the image processing module. Therefore, the functions used for textural feature extraction have to be fairly simple and straight-forward, while at the same time very economic in storage resources.

A very attractive option for future improvements of the current design is the introduction of new, more efficient, textural feature extractors within the same image processing framework. Specifically, instead of using only first-order statistics from the histogram of the current image sample, second-order statistics could also be used [B01]. Second-order statistics that are based on greylevel co-occurrence matrices of the image have been applied successfully in a wide range of medical and geographical applications [B02]. Furthermore, another option similar to these feature functions is the employment of run-length statistics, proved to be equally useful and powerful in terms of image texture analysis in medical or other applications [B03].

The usefulness of both second-order greylevel statistics and run-length statistics is based on the fact that they exhibit very robust and consistent behavior on various types of texture. Specifically for medical applications, they are better fit for recognizing homogeneous areas of tissue than the first-order statistics, while at the same time they are able to capture information content and discrimination attributes within the underlying image with much better quality.

The implementation of second-order or run-length statistics requires one additional level of abstraction within the image processing module, i.e. the calculation of spatial co-occurrence matrices of the greylevels, before the actual textural features can be calculated. This is a time-consuming and storage-demanding task that creates additional requirements for the sensor IC design. However, modern ASIC options, especially FPGA, could enable the introduction of similar options with minimal deviations from the design and cost of the current sensor IC of the prototype I-ImaS system.

6.4.2 Advanced pre-filtering – on-line image restoration

The quality of the extracted textural features is directly related to the quality of the raw data of the primal image. This means that if the primal image, formulated by the first “scout” scan can employ a quality level that enables a robust extraction of content-related information, then the subsequent estimation of the quality and the required exposure adjustments will be much more efficient.

The two main factors affecting the quality of the primal X-ray image are the channel distortion and the cumulative noise factors [B04]. Channel distortion includes all the degradation effects introduced by the system itself, including the flat-field correction (black and white), the fixed spatial resolution and the moving sensor plate. The noise factors include mostly X-ray scattering and sensor efficiency. Image restoration deals with both these issues by estimating a top-level model of the channel distortion, in the form of a digital filter, and subsequently applying a statistically "inverse" filter, in order to cancel or at least limit the effects of these distortions in the final image [A04].

Section 8.1 describes the issue of image restoration in the context of image post-processing, i.e. using off-chip computing resources. Generally, the estimation and application of a detailed and robust image restoration model requires significant amounts of computing resources due to the complexity of the underlying algorithms. Therefore, they are usually applied only in post-processing stages, where the time-critical property is usually not an issue. However, if such an approach can or has to be realized within the context of the on-line processing, as for example in audio channel equalization, then the acquisition and pre-processing stages of the control loop produce incoming data of much better quality. In the context of I-ImaS, such an on-chip implementation could greatly benefit the efficiency of the control module itself, as the automatic image quality assessment, on which the feedback decision is based, would be much more realistic.

6.4.3 Full state-space description – iterative models

As mentioned in sections 6.1.1 and 6.1.2, a realistic derivative estimation of the transition plane in the quality index space requires several instances (calculations) of the state-variables vector at different input settings. This means that, in order to calculate the local transitions of extracted textural features, several instances of these features would have to be calculated on the same tissue area, using slightly different exposure parameters. The current I-ImaS design for sensor IC does not permit varying exposure parameters within the same "scout" scan, as it assumes constant exposure levels during this phase.

An iterative approach could employ such a design for the sensor IC, providing 2 or 3 different exposures over the same tissue area, as a multi-step "scout" scan. The different samples or "versions" of the primal image would be used to estimate the local slope in the transition plane in the quality index space and, subsequently, the local gradient of the quality index. This way, no external "a priori" knowledge of the transition plane in the quality index space would be required and a much more accurate estimation of the required feedback could be calculated.

The same approach could be extended for the second "adapted" scan as well. Instead of allowing only one step of adjustment, the feedback could be calculated for a localized quality improvement towards the optimal gradient. Thus, an iterative quality optimization would produce much more accurate and efficient feedback for the required exposure level, at the cost of significantly more complicated "scout" scanning and non-trivial adaptive control calculations.

6.4.4 Causal state-space description – recursive models

The notion of multiple samples or "versions" of the primal image during the first scout scan and/or during the second "adapted" scan can be extended in a generalized version of the quality estimation procedure. In practice, this is equivalent to exploiting the optimization results of the previous N-1 steps to produce the next step towards the intended purpose. These systems are called "causal" and their implementation results in recursive processing models.

The Kalman filtering technique is of fundamental importance in linear estimation theory [C01]. According to Kalman models, a linear state-variable system similar to

the one introduced in section 6.1.3 can be associated directly with the statistics of the incoming data. Kalman filtering requires a stochastic model of the quantity to me estimated, whereas the Wiener filters are totally based on the knowledge of auto-correlation and cross-correlation matrices of the observed data [A04]. This means that they provide the means to implement recursive realizations of the corresponding control filters, not based on the complete or previously known statistics of the data, but instead using the subsequent observations as the data arrive sequentially. In the context of the I-ImaS sensor IC, this is equivalent to using the statistics of the *gradually improving* primal image samples in order to calculate the appropriate adjustments as feedback for acquiring an even better primal image in the next scan.

The employment of Kalman filters in the control loop can be realized either in the form of one-step predictor for the next state-variables vector or by a direct association to the estimated image quality. In the first case, the system reduces to a simple k-tap linear predictor [A06] that estimates the next resulting textural feature values, which can be applied for a more accurate estimation of the combination formula for the image quality function (Eq.6-12). In the second case, the system is a full state-space description, in direct accordance to the state-space model introduced in section 6.1.3, only not the process is calculated in a recursive manner.

Either way, the storage requirements of the Kalman filters are lower than Wiener equivalents, yet the computational complexity may still be prohibiting for implementing them as embedded on-chip functionality [A06]. However, if such an approach would be feasible in the context of the current or future designs of the I-ImaS sensor IC, *the necessity of using dual scan could be reassessed, as in this case the recursive filtering model would essentially exploit the "history" of previous single scans* in order to decide on the next feedback.

6.4.5 Non-linear control – neural & fuzzy models

Thus far, a linear state-space model was assumed for the description of the control model, incorporating additive linear factors for the current texture feature values and the current exposure settings for the calculation of the required feedback. As Fig.6-2 illustrates, the control loop actually includes a two-stage linear control module, one for estimating the resulting image quality index and one for translating the difference between quality indexes (current versus required) into differences between exposure settings (adjustment/feedback).

In practice, many cases require much more complex associations between the input and the output. If either the textural features response curve versus dose or the experts' quality assessment versus dose cannot be approximated with acceptable error by a linear regression function, the linear state-space description presented in section 6.1.3 and so on becomes invalid. In this case, a more general approach is required, similar to the state-space description model presented in section 6.1.2 (for stationary systems) or the model presented in section 6.1.1 (for non-stationary systems).

Modern automatic control often needs to exploit current state-of-the-art digital technology in order to realize extremely complex control patterns. In this case, linear modules can be substituted by off-chip powerful computing equipment or even implement some of their functionality on-chip in order to achieve more "intelligent" response functions. Two of the most common approaches are the neural networks and the fuzzy controllers.

Embedded neural network controllers [C02], although not very common in consumer applications, can be implemented in the form of firmware or even in hardwired solutions, using digital or analog processors. Their performance is usually related to their size and topology, which means that complex control plans usually require proportionally complex topologies. Neural networks are hosted in

programmable storage matrices in the form of weights (digital or analog) and their on-line functionality is usually a direct “forward-flow” of the incoming data, similar to a typical filter. The weights of the network are calculated off-line independently from the actual operation of the system, during a “training” phase that exploits arbitrary relationships between input and output samples.

Fuzzy controllers [C03] have become increasingly popular during the last decade, mostly by the introduction of new powerful digital processing modules that could incorporate combinations of partially linear or window-like activation functions. The most typical form of fuzzy control is the design of several operational conditions in the form of an optimal response profile (ORP – see section 5.2), which implements a detailed top-level state-transition model for the system, and an optimal control profile (OCP – see section 5.2), which realizes the appropriate transitions according to the required behavioral plan. Usually, the fuzzy controller approach is applied when a detailed behavioral plan is available, e.g. through a rule-based description from an expert, or when a more time- and storage-consuming solution (like a neural network) cannot be employed.

Both neural and fuzzy approaches provide the means for implementing highly sophisticated response to the system, the first by automatically “discovering” the inherent complex relationships between the input and the output, and the second by robust and economic realization of a top-level description of a behavioral plan. Fuzzy controllers are usually more economic in terms of required resources and speed, mostly because of the simplicity of their internal structure. Embedded neural network controllers are best suited for applications where there is an increased level of required fault-tolerance, resilience to noise in the input, as well as in cases where there is no top-level description of the expert’s knowledge or when the system itself is highly temporal.

In the context of I-ImaS, a fuzzy or neural controller could easily substitute the quality index assessment module (Fig.6-2, first stage), as well as the feedback estimator (Fig.6-2, second stage), into one combined node in the control loop. The utility of such a choice should be measured in relation to the true efficiency of a simpler linear solution, as well as the accompanying cost in the final system.

7. Pre-processing phase

The raw data extracted from the detector need to be corrected in order to use them to extract the interesting textural features needed for image evaluation.

In particular, the data are generally affected by fixed pattern disuniformities caused by:

- photon absorption changes due to fluctuations in the phosphor thickness and variations in the size of the sensitive region of the IC, both due to the manufacturing process. The beam projection geometry can also determine a disuniform photon absorption in the detector depending on the position in the image;
- light collection efficiency disuniformities due to the phosphor deposition techniques and defects in the coupling with the silicon sensor;
- charge collection efficiency disuniformities due to the IC manufacturing process;
- readout electronics reset level, dark current and gain fluctuations in the Analog to Digital conversion.

In an integrating front-end electronics, like the one used by I-ImaS, these disuniformities can usually be corrected linearly and there is no dependency from the photon fluency.

The fixed pattern correction can be modeled as following:

$$X = R/G - (N\_0+I\_0*t) \qquad \text{[Eq.7-1]}$$

where X is the corrected read out of the pixel, R is the raw data, N_0 the reset level, I_0 the dark current, t the exposure time and G the gain correction. The contribution of N_0 and in particular I_0 is expected to be negligible, while it is still impossible to determine which will be the order of gain disuniformities.

"Dead" or saturated pixels will also be corrected by calculating the mean of the closest detector elements.

Other pre-processing algorithms (edge enhancement, histogram equalization, spline correction) have been tested on digital images acquired with a CCD and an image plate, but they showed no advantages in order to extract interesting textural features, and in some cases the results were deteriorated [A01].

8. Post-processing phase

8.1 Image restoration

As in any image acquisition system, the quality of the input data are expected to exhibit e certain degree of *degradation*, mostly due to the design, functionality and deficiencies of the detecting system, as well as the overall additive noise effects. Image restoration is concerned with filtering the observed image to minimize the effects of these degradations, thus resulting in the best approximate of the theoretically “perfect” image. It is fundamentally different from image enhancement, in the sense that the later is mostly concerned about the improvement of any extracted image features, rather than the restoration of image degradations during the acquisition process [A04].

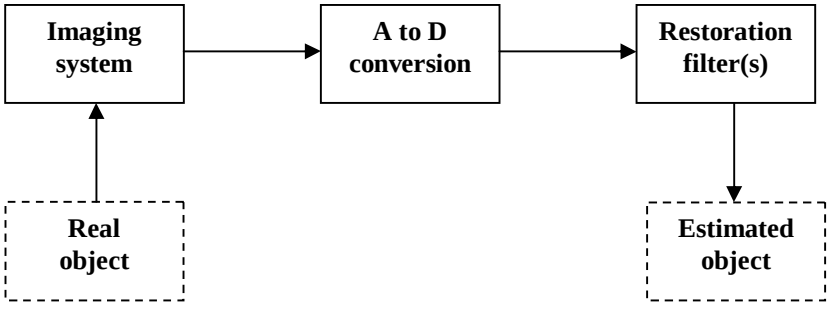

Figure 8-1: Image restoration block diagram.

The effectiveness of image restoration filters depends on the extent and accuracy of the knowledge of the degradation process, as well as the filter design criterion. The most commonly used optimization criterion is the mean square error of the initially acquired image versus the one predicted by a solid theoretical model if no degradations were present. Usually, this is achieved by first modeling the true response of the acquisition system, using a mathematically modeled test pattern

phantom image, and subsequently using the "inverse" form of the evaluated model as a post-processing filtering module.

This section presents some of the most prominent options for implementing image restoration stages in the post-processing phase of the I-ImaS system. After a brief description of image observation models and their analogies to the I-ImaS system, the general framework of inverse and Wiener filters is presented in the context of image restoration applications. Furthermore, some alternative options are discussed for specific applications, possibly useful for the final prototype of the I-ImaS post-processing imaging software.

8.1.1 Image observation models

A typical imaging system consists of an image formation system, a detector and a recorder. In the case of I-ImaS, the image formation system and the detector are fused into one module, i.e. the X-ray sensor plate, while the image recorder is implemented in the form of digital registers, also within the sensor IC. All the acquired data are fed directly into the digital registers for further processing, which essentially constitute the input data source for the rest of the system. Therefore, as far as image restoration is concerned, the sensor IC is a "black box" that incorporates the complete response of the image acquisition system.

An additional property that affects the quality of the acquired data is the overall noise effects. In X-ray imaging, these effects are usually the result of detector inefficiencies, electronic interference, as well as beam scattering in the system and the target object itself. The resulting noise, although difficult to model in its final form, can be estimated as a contributing factor on the resulting image by means of estimating certain statistical properties within special well-defined areas of the projected plane. In case of Gaussian noise model, which is the most common case for complete noise estimation, the signal variance over homogeneous image areas can be a statistically solid measurement of noise power. In case of multiplicative noise, the complete noise model becomes a sum of two separate noise factors, namely η_1 for the multiplicative term and η_2 for the additive term:

$$\eta(x,y) = \sqrt{g(x,y)} \cdot \eta_1(x,y) + \eta_2(x,y) \qquad \text{[Eq.8-1]}$$

Noise type	Grayscale histogram model	Application
Gaussian	$H_N(g) = \frac{1}{\sqrt{2\pi\sigma^2}} \cdot e^{-(g-m)^2 / 2\sigma^2}$	General noise model for unknown or additive noise effects
Uniform	$H_U(g) = \frac{1}{g_{\max} - g_{\max}}$	General noise model for uniform processes

Salt & Pepper	$H_{SP}(g)=\begin{cases} A & , \quad g=a\{"pepper"\} \\ B & , \quad g=b\{"salt"\} \end{cases}$	"Black" and "white" pixel inconsistencies due to detector inefficiencies
Rayleigh	$H_R(g)=\frac{2g}{a}\cdot e^{-g^2/a}$	Noise model in radar range and velocity images
Negative Exponential	$H_{NE}(g)=\frac{e^{-g/a}}{a}$	Noise model in laser-based sensor images
Gamma	$H_G=\frac{g^{a-1}}{(a-1)!\cdot a^a}\cdot e^{-g/a}$	Noise model for low-pass filtered laser-based sensor images

Table 8-1: Noise models and their applications in image processing [D01].

From the various types of noise models and their applications presented in Table 8-1, the two most prominent ones for implementation within the first post-processing stages of the I-ImaS image acquisition system are the Gaussian and the Salt & Pepper. The Gaussian is most suitable for a generalized noise model that can be easily combined with most image restoration filters, including Inverse and Wiener filters, while the Salt & Pepper noise model can be introduced as the very first stage of the post-processing phase in order to cope with typical random "bad" pixels in the acquired X-ray image.

In I-ImaS, the specific architecture of the line-scanning procedure adds a significant factor in the image acquisition process. The relative movement of the complete sensor IC against the projected tissue area that is recorded results in a "motion blurring" effect that degrades the resulting image.

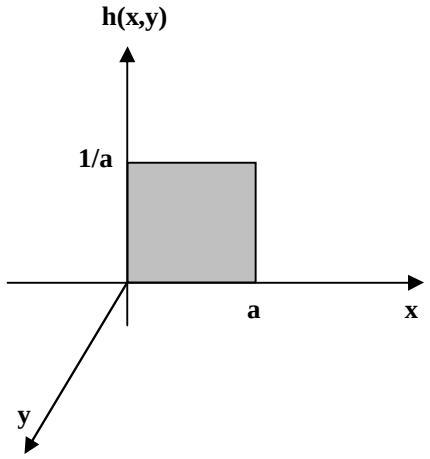

Figure 8-2: Point-spread function (PSF) of uniform 1-D motion blurring [A04].

Type of system	Impulse response ***h(x,y)***	Frequency response ***H(ξ1,ξ2)***
Horizontal motion (x-axis)	$\frac{1}{a_0}\cdot rect\left(\frac{x}{a_0}-\frac{1}{2}\right)\cdot\delta(y)$	$\mathrm{sinc}(\alpha_0\xi_1)\cdot e^{-j\pi\xi_1\alpha_0}$

Rectangular scanning aperture integration	$rect\left(\frac{x}{a},\frac{y}{b}\right)$	$ab\cdot\mathrm{sinc}(\alpha\xi_1)\cdot\mathrm{sinc}(b\xi_2)$

Table 8-2: Spatially invariant formulation of scanning 1-D and 2-D models [A04].

The specifics of this motion effect can be theoretically predicted by the exact specifications of the line-scanning system, as Figure 8-2 and Table 8-2 illustrate. However, these theoretical formulations can be implemented in the form of a *separate* filtering stage only when the complete response of the image degradation model can be safely characterized as separable [A04]. This means that if the "motion blurring" effect is considered statistically independent of any other type of degradation, including noise and detector inefficiencies, then it is possible to design a reverse filtering module that essentially cancels this specific degradation process [D30,D31].

8.1.2 Inverse and Wiener filtering

Inverse filtering is the process of recovering the input from its output. In the absence of noise, the *inverse filter* of an acquisition system is the one that compensates the effects of this system's impulse response, thus canceling any degradation effects of the input data. In frequency domain, the inverse filter can be calculated by the mathematical inverse of the identity formula:

$$H_{inv}(\omega_1,\omega_2)\cdot H(\omega_1,\omega_2)=1 \quad\Leftrightarrow\quad H_{inv}(\omega_1,\omega_2)=\frac{1}{H(\omega_1,\omega_2)} \qquad \text{[Eq.8-2]}$$

According Eq.8-2, the spatial domain convolution kernel of the inverse filter can be calculated by the inverse Fourier transform of the mathematical inverse of the frequency response of the system. However, there is no guarantee that the divisor in Eq.8-2 is non-zero. In fact, for values close to zero and at low noise levels, the inverse filter of Eq.8-2 becomes highly unstable and produces overflow effects, thus destroying the otherwise restored image. A stabilized version of the typical inverse filter is the *pseudo-inverse* or *generalized inverse filter*:

$$H_{pinv}(\omega_1,\omega_2)=\begin{cases}\dfrac{1}{H(\omega_1,\omega_2)} & , \quad H\neq 0\\ 0 & , \quad H=0\end{cases} \qquad \text{[Eq.8-2]}$$

The pseudo-inverse filter is mathematically well-defined under all conditions, but it still remains highly sensitive to additive noise and/or round off errors, since low noise levels in the initial image are effectively amplified by both the inverse and the pseudo-inverse filters [A04,B04].

A more robust category of restoration filters can be built upon the general theory of *Wiener filters* [A04,A06]. Wiener filtering is a method of restoring images in the presence of a system's characteristic response convolution as well as noise effects. When applied to images, it produces the statistically optimal estimate of the original image according to a probabilistic model for the source data. The best

estimate of the original image is the conditional mean against the acquired (degraded) image:

$$\sigma_{err}^2 = E\left[\left(o(x,y) - \tilde{o}(x,y)\right)^2\right] \qquad \text{[Eq.8-3a]}$$

$$\tilde{o}(x,y) = E\left[o(x,y) \mid d(k,l), \quad \forall(k,l)\right] \qquad \text{[Eq.8-3b]}$$

where *o(x,y)* is the recorded object and *d(x,y)* is the degraded version of *o(x,y)*. The impulse response of the restoration Wiener filter is calculated from Eq.8-3b such that the estimation error in Eq.8-3a is minimized. When Gaussian distribution is used in the probabilistic model, the equations Eq.8-3a/b reduce to a set of simultaneous linear equations that can be used to calculate the required frequency response of the Wiener filter, also called the Fourier-Wiener filter:

$$G(\omega_1,\omega_2) = \frac{H^*(\omega_1,\omega_2)\cdot S_{oo}(\omega_1,\omega_2)}{\left|H(\omega_1,\omega_2)\right|^2 \cdot S_{oo}H(\omega_1,\omega_2) + S_{\eta\eta}H(\omega_1,\omega_2)} \qquad \text{[Eq.8-4]}$$

where G is the filter's frequency response, H^* is the complex conjugate of the system's frequency response function and S is the power spectral density functions for the recorded object and the noise.

Generally, the Wiener filter is not separable even if the PSF and the various covariance functions are [A04]. This means that it can not be applied row-by-row and subsequently column-by-column, similarly to the FFT transformation. However, the zero-mean model defined by Eq.8-4 can be easily extended to non-zero mean images, simply by introducing the statistical mean values of the corresponding object and noise data into the mathematical model:

$$\mu_d(x,y) = h(x,y) * \mu_o(x,y) + \mu_\eta(x,y) \quad , \quad \mu_k = E[k] \qquad \text{[Eq.8-5a]}$$

$$\hat{d}(x,y) = h(x,y) * \hat{o}(x,y) + \hat{\eta}(x,y) \quad , \quad \hat{k} = k - \mu_k \qquad \text{[Eq.8-5b]}$$

According to equations Eq.8-5a/b, the non-zero mean version of the Fourier-Wiener equations become:

$$\tilde{O} = G\cdot(D - M_d) + M_o = G\cdot D + \frac{S_{\eta\eta}}{\left|H^2\right|\cdot S_{oo} + S_{\eta\eta}}\cdot M_o - G\cdot M_\eta \qquad \text{[Eq.8-6]}$$

where M denotes the Fourier transform of the mean. The model described by Eq.8-6 allows spatially varying means for both the recorded object and the noise, which can be calculated by local averaging over a fixed sampling region size. In case of constant means, the Fourier equivalents also become constants in the form of Dirac delta functions that can be easily calculated [A04]. In any case, for zero or low levels of noise, the Wiener filter reduces to the inverse or pseudo-inverse filter, accordingly, compensating a low-pass smoothing response on the acquisition system with a high-pass frequency response on the restoration filter. In the presence of significant noise, the Wiener filter ensures the best compromise

between high-pass filtering and reduced noise amplification, in the form of a band-pass frequency response.

Theoretically, the Wiener filter has infinite impulse response which requires working with large size FFT transformations and convolution kernels. However, the effective response of these filters is usually much smaller than the object size, thus optimum finite impulse response (FIR) filters can be realized with acceptable performance and significantly lower computational complexity. When Wiener models are designed as FIR filters, the specifications described by Eq.8-3a/b reduce to a set of simultaneous linear equations in the form of:

$$r_{od}(x,y) - \sum_{i \in W} \sum_{j \in W} \left[g(i,j) \cdot r_{dd}(x-i, y-j) \right] = 0 \quad , \quad \forall (x,y) \in W \qquad \text{[Eq.8-7]}$$

where (r_{dd}) is the auto-correlation function of the observed image object and (r_{od}) is the cross-correlation function between the observed image object and the theoretically expected object projection, over a kernel of size W, *generally proportional to the width of the PSF of the acquisition system* [A04]. Equation Eq.8-7 describes a set of $(2M+1)^2$ linear equations that can be calculated easily over an NxN sampling region over the acquired image, where M is the size of the Wiener filter and N is the size of the sampling box. The required size of the filter increases with the amount of blur and additive noise introduced by the image acquisition system. If the system's PSF leads to a filter size of at least M pixels, then the sampling box should be at least N=2M accordingly, as correlations outside this support area can be considered negligible.

In order to obtain the final model for the I-ImaS restoration filter, a spatially variant version of the FIR filter has to be formulated. Since the line-scanning system may incorporate non-uniform sensor IC movement in micron level, non-uniform X-ray beam geometry due to varying deflection angle, or possibly non-uniform noise distribution over the entire scanning area, the resulting PSF may not be constant, thus resulting in spatially non-stationary images. A simple but effective non-stationary model for images incorporates spatially varying mean and variance functions and shift-invariant correlations. In this case, the Wiener filter response also becomes a spatially varying function:

$$\hat{g}_{x,y}(i,j) = g_{x,y}(i,j) + \frac{1}{(2M+1)^2} \cdot \left[1 - \sum_{i \in W} \sum_{j \in W} g_{x,y}(i,j) \right] \qquad \text{[Eq.8-8]}$$

The second term in Eq.8-8 adds a constant with respect to (i,j) to the FIR filter, *which is equivalent to adding to the estimate a quantity proportional to the local average of the observations*. Common realizations of these types of spatially varying Wiener filters are the Optmask [D08] and the Cosar filters [A04].

If the system's impulse response is quite complex and the resulting filter response is too time-consuming to implement in the spatial domain as a 2-D convolution, the Wiener filter can be calculated in the frequency domain, sampled over a NxN grid and then applied on the Fourier transform of the current image sample, hence resulting in a filtered version of the image in the frequency domain. If advanced FFT or convolution IC modules are available, then the implementation can be realized directly in the sensor IC, i.e. in hardware, for on-line processing.

For I-ImaS, the complete restoration filter can be realized as a non-zero mean spatially varying Wiener filter, using a custom set of test pattern phantom images that can be applied for calibrating the system off-line (see section 9).

8.1.3 Other filter options

The Wiener filters are not the only options suitable for image restoration applications. Other options for estimating optimal restoration filters include Kalman filters, geometric mean filters, generalized Wiener filters, homomorphic Wiener filters, fast decomposition filters, as well as least-squares and iterative methods.

Kalman filters [C01,A06] are a very robust causal alternative to the state-space description methods, already discussed in section 6.3.4 in relation to the I-ImaS control model. Kalman filtering requires a stochastic model of the quantity to me estimated, whereas the Wiener filters are totally based on the knowledge of auto-correlation and cross-correlation matrices of the observed data [A04]. Thus, the Kalman filters are well-suited for applications where the available computational and storage resources are limited, as in the case of on-line processing.

The *geometric mean filter* combines the pseudo-inverse and the Wiener filter, using an additional exponential parameter. This parameter can be defined in such a way that, unlike the typical Wiener filter, the power spectral density of the output is identical to that of the object under all conditions [A04].

The *generalized Wiener filter* is a typical formulation of the standard Wiener filter, in a way that permits a more efficient and fast approximation. Specifically, the incorporation of fast unitary transforms permits the algebraic decomposition of the related matrices into a reduced set of equations, such that the effective size of the required calculation kernels are much smaller than that of the full model, in the scale from $O(M^6)$ to $O(2M^2 logM)$ [A04]. This implementation is possible when the filter matrix can be diagonalized exactly or approximately.

When the noise is multiplicative in nature, rather than additive, then logarithmic transformation can be applied on the input data, followed by the corresponding exponential inverse on the output data. Thus, the resulting Wiener filter incorporates additional pre- and post-processing steps, and the new formulation is called *homomorphic Wiener filter* [A04,D01].

For narrow PSF functions and stationary observation models, the filter matrix can be decomposed into a sum of two matrices, where the first one can be diagonalized and the other is a composition of the system's frequency response and a sparse matrix of low rank. In that case, the filter can be realized as a generalized Wiener filter, with the additional computation of low-order matrix decomposition operations. This type of filters are often called *fast decomposition filters* [A04]. The exact number of these operations depends on the exact width of the PSF and the image correlation model.

If direct least squares optimization is used to achieve the optimal restoration result, the finite Laplace operator, i.e. the sum of the directional derivatives, can be used as a "roughness" index over a fixed grid. Subsequently, a *constrained least squares filter* formulation can be described for the filter output and the restored image is estimated directly as the outcome of the optimization process [D18,D19,A06].

An optimization formulation can also be realized through an iterative process, using gradient methods. When the aim of the solution is to obtain the restored image itself rather than the restoration filter, then the *one-step gradien*t method can be used [A04]. A more efficient realization of this type of optimization is the *conjugate gradient method* [D22,D23,D24], which incorporates adaptive step and theoretical upper bound for the required iterations, usually limited to less than the rank of the system's frequency response matrix. In case of narrow PSF functions, additional enhancements can lead to even more efficient implementations.

8.2 Visualization

The resulting images of the developed intelligent sensor will consist of regions with different exposure settings which results in square patterns over the images. For radiologist to analyze the new regulated x-ray images, a visualization algorithm is needed to make the images transparent of which local exposure settings used. The developed algorithm is made of a global model for the correction based on a set of calibration images, followed by a local adjustment based on the image alone.

The visualization algorithm is developed using the mammography tissue images from database DB3 consisting of 4 images sets (U01, U02, U03, U04).

8.2.1 Linear visualization correction model

We have made a model fitting a 1st order polynomial (y = Ax+B) for each jump in mAs value for one specific kVp value (here kVp = 30). That means that if we want to show the mammography image as an image captured with mAs = 40 and kVp = 30. We need a mapping for each mAs value in the original image to mAs = 40. Figure 8-3 shows the linearity for intensity mapping from mAs = XX to mAs = 40 for image set U04. In Figure 8-4 we show how the coefficients (A and B) are a function of the mAs value mapped to mAs = 40. We see a clear exponential relationship with mAs.

The entire image is used for making the calibration parameters. The resulting parameters are used when mapping the intensity values. The mapping could also have been realized as a look-up table.

Image set U03 and U04 shows linear relationships, while image set U01 and U02 deviate some from this assumption. This will probably be the case when the background and foreground has different mappings.

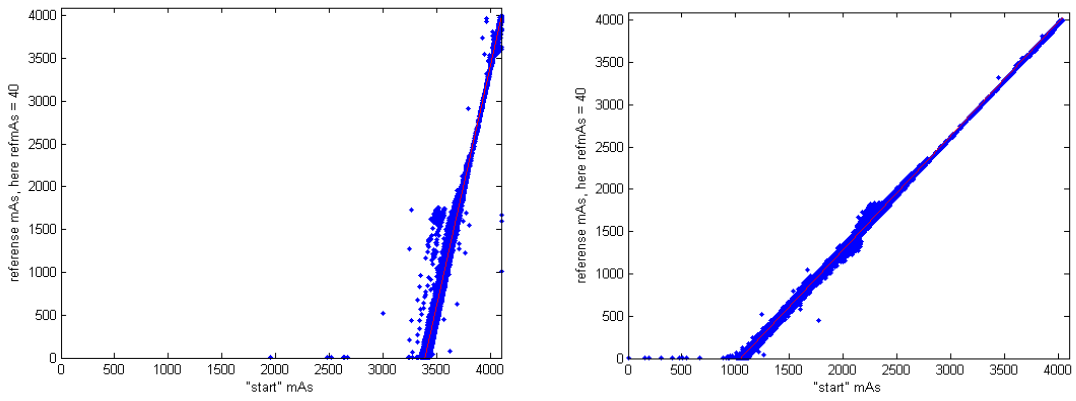

Figure 8-3: Input mAs = 4 (left) and 25 mAs (right).

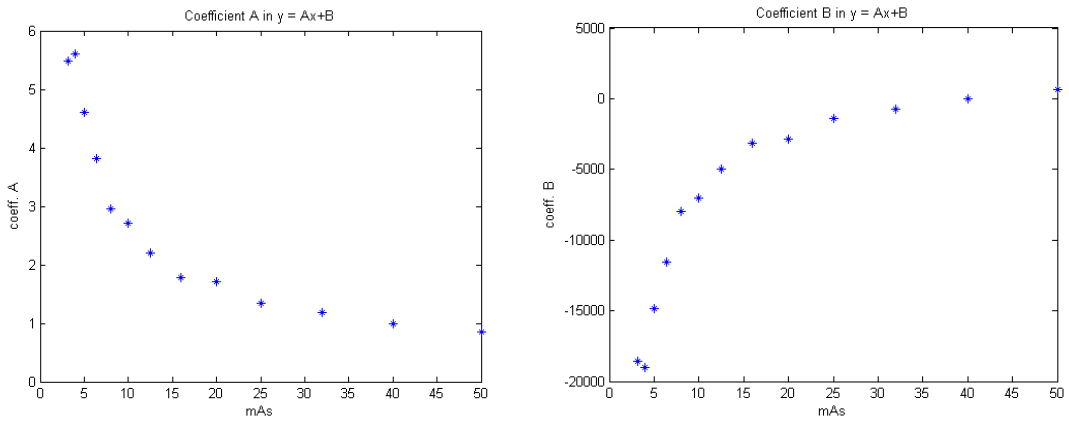

Figure 8-4: The coefficients in the fitted conversion of intensity at one mAs to a reference mAs images (40mAs), as a function of mAs.

We have made a visualization model for each of the image sets (U01, U02, U03 and U04) and used these models to visually correct the regulated images. When applying the model and the regulated image from the same image set we get a very good result, as expected. However, when we apply a model made from another image set some deviation occur.

Global correction of regulated images from U03 and U04 are shown in Figures 6-5 to 6-8.

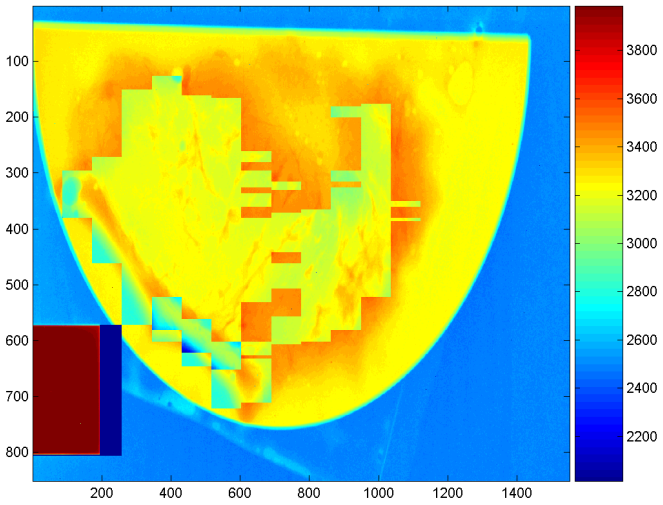

Figure 8-5: Simulated regulated image U03 for kVp equal 28.

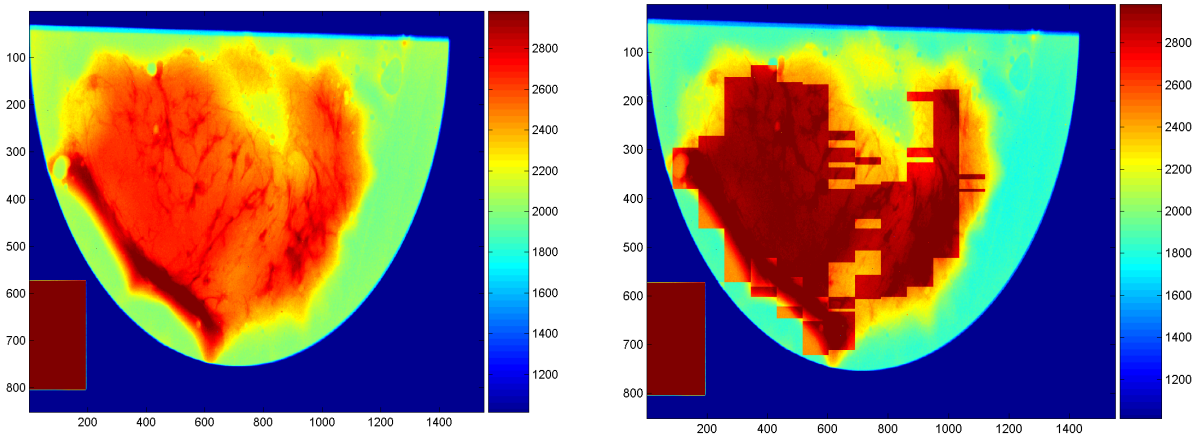

Figure 8-6: Global visualization corrected image U03 applying parameters from U03 (left) and applying parameters from U04 (right).

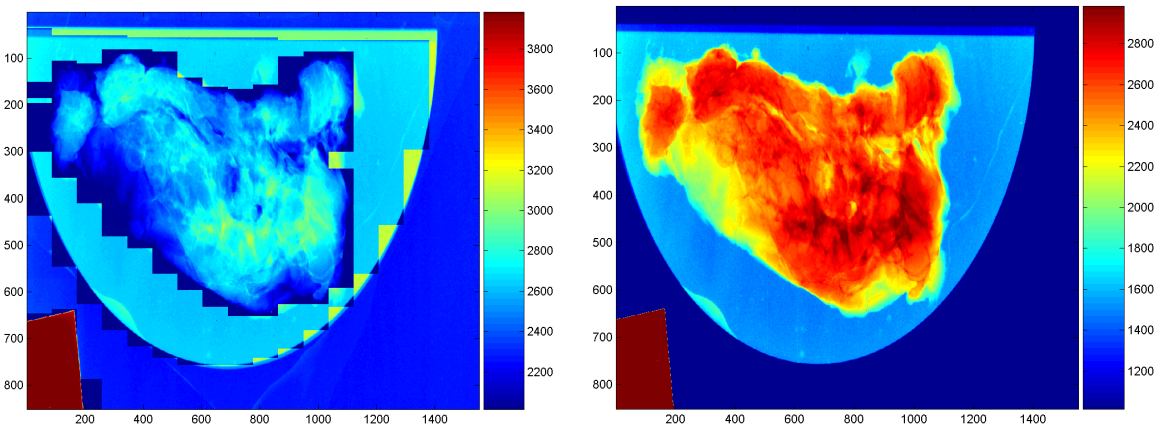

Figure 8-7: Regulated image U04 (left) and global visualization corrected U04 image with parameters from image set U04 (right).

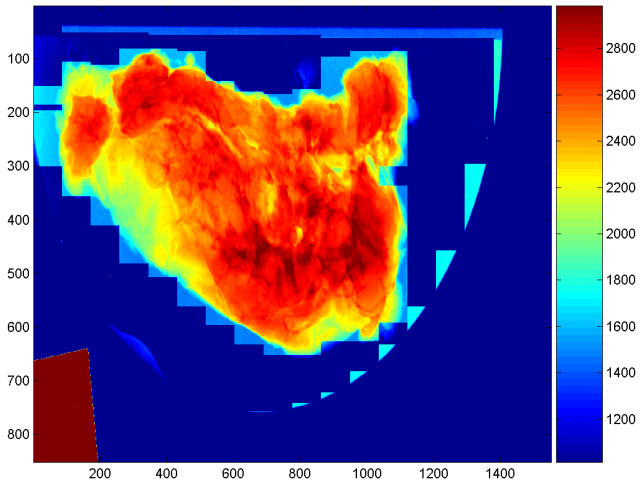

Figure 8-8: Global visualization corrected U04 image with parameters from image set U03.

In Figures 8-9 to 8-10 plots of the conversion parameters are shown as a function of mAs. We see that the differences in parameters are as large between kVp-values as between samples. The exponential relationship is not at smooth for all samples. Image set U01 shows the best exponential curve as a function of mAs.

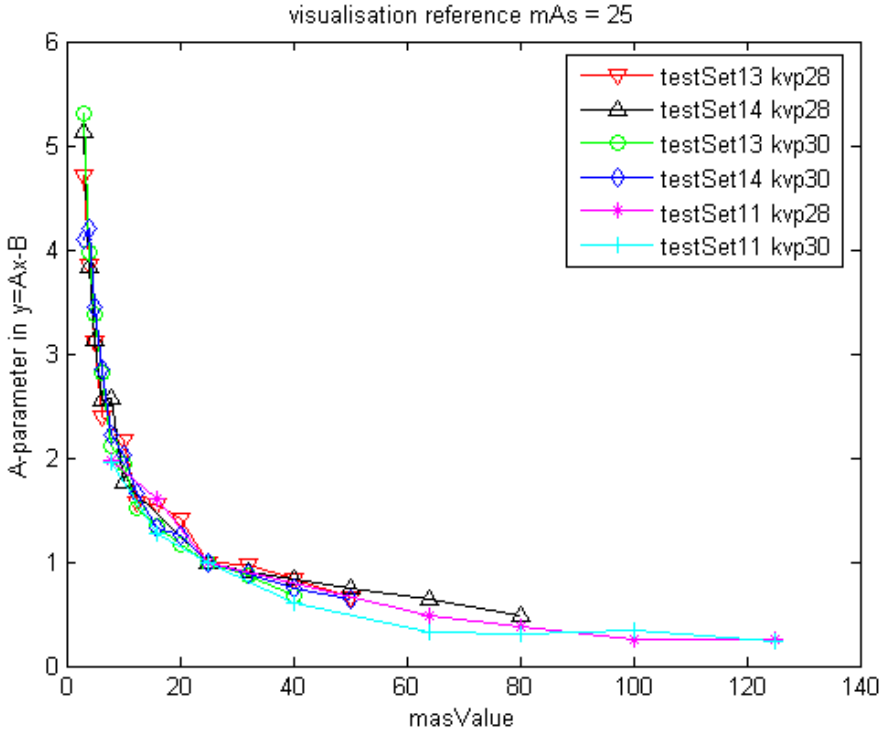

Figure 8-9: Parameter A as function of mAs, when reference mAs = 25.

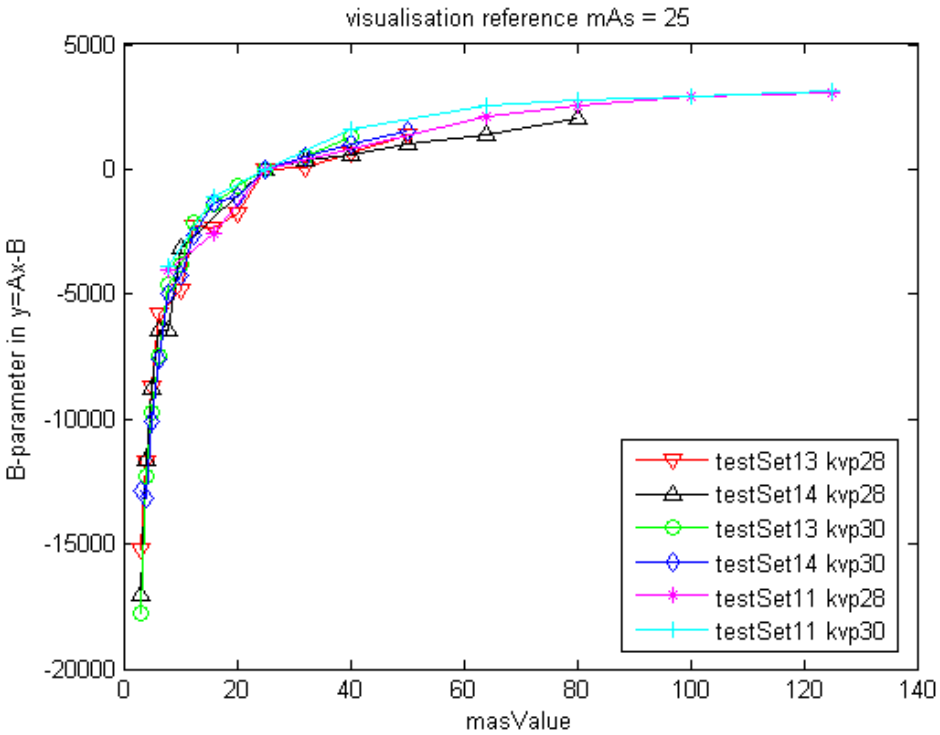

Figure 8-10: Parameter B as function of mAs, when reference mAs = 25.

8.2.2 Local intensity adjustments

Since there are some deviations in the parameters from the different image sets and the parameter curves are not smooth an additional local adjustment algorithm is developed.

To make a local adjustment we have used the mAs image to find all transitions from one mAs value to another. We then pick out the area with the highest mAs as the reference and adjusts all the other mAs areas toward these values. We use all transition rows from one mAs to another and find the pixel wise difference.

We can see from the plots in Figure 6-13 that we for some of the mAs transitions have a linear relationship between the greyscale value in the lowest of the two mAs values and the neighbour pixel differences. By actively using this when doing the local adjustments we will improve the visualization, see Figures 6-11 and 6-12. We have used the pixel intensities in the lowest of the two mAs values since this is the intensity values to be adjusted.

All pixels in the global model corrected image with intensity values zero (0) is also set to zero (0) in the locally intensity adjusted image.

The user can also make a chose to run a mAs edge smoothing. This means that the pixels at and adjacent to the mAs transitions are smoothed with a mean filter to blur out any intensity shifts at the transitions. We have chosen the default filter sizes 3x3 for horizontal edges and 5x5 for vertical edges.

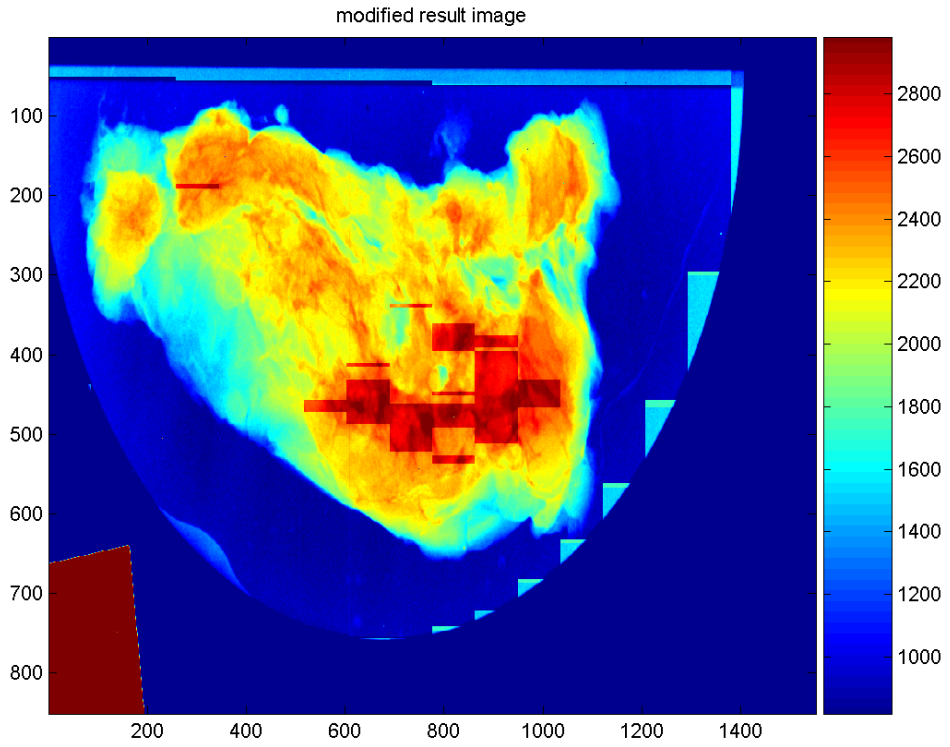

Figure 6-11: The global model adjusted U04 image using parameters from U03.

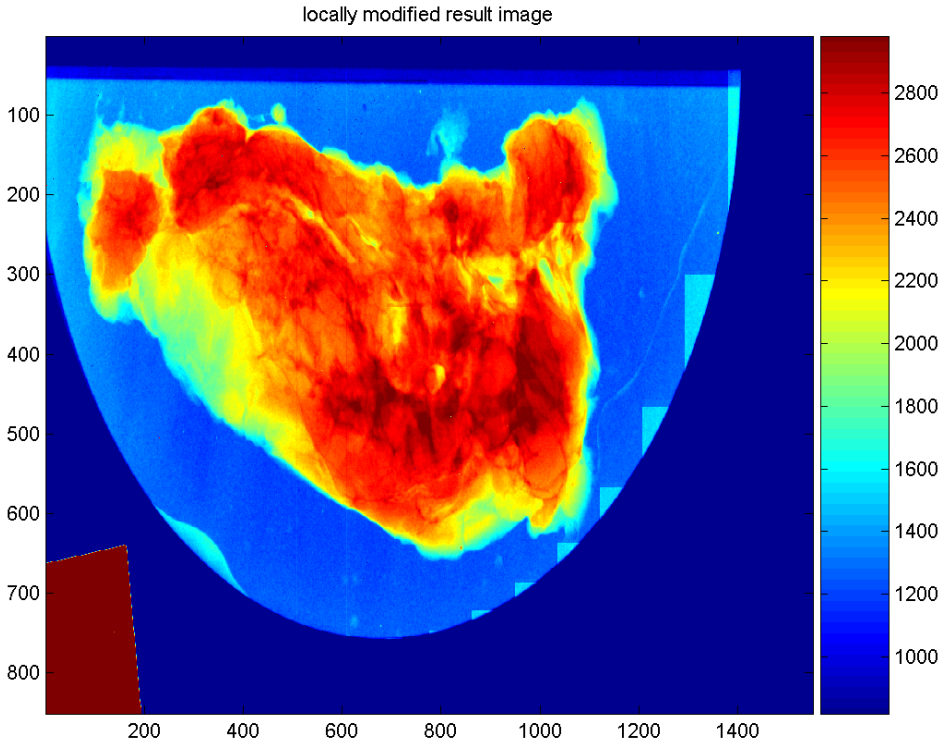

Figure 6-12: After the image in Figure is locally adjusted.

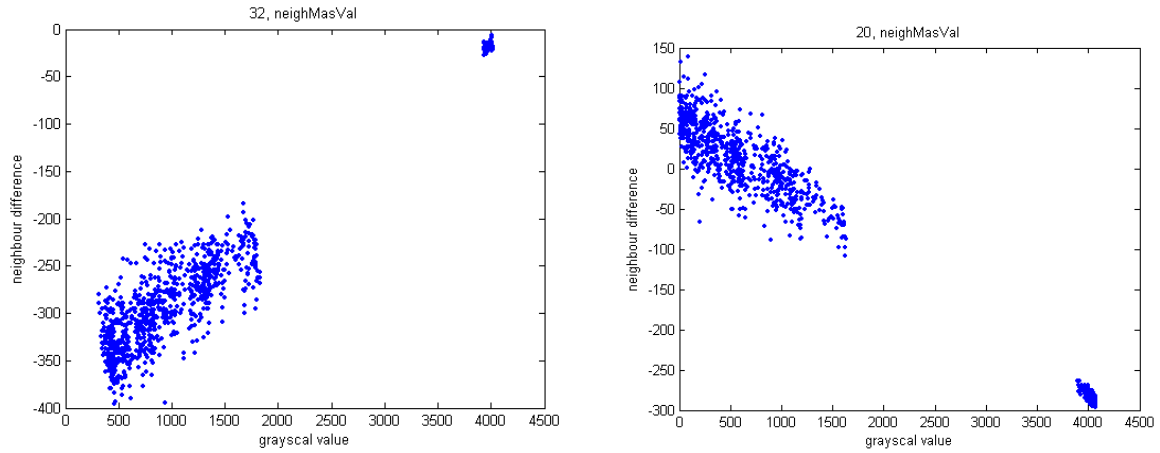

Figure 6-13: Pixel difference between mAs 40 and 32 and mAs 25 and 20 in test set 13, kVp = 30.

9. System Calibration

The I-ImaS acquisition system incorporates a pre-processing phase, including some basic on-line image enhancement processing, and a post-processing phase, including sophisticated off-line image restoration process. Additionally, the exposure control model has to be partially initialized with some parameters related

to the dynamic range of the grayscale. For acceptable performance and within the required operational profiles, the system has to be *calibrated* though a series of well-defined procedures that estimate the required internal model parameters.

This section describes the details regarding the calibration procedures and supporting test data, including the pre-processing phase (9.1), the control module (9.2) and the post-processing phase (6.3).

9.1 Pre-processing modules

The raw data acquired by the detector will be corrected from fixed pattern disuniformities. The parameters G, N_0, I_0 used in equation (7.1) will be estimated by fitting dark field images, while G will be estimated from flat field images.

For these purpose the calibration procedure will consist of acquisitions of:

► *Dark field images* with different exposure time in order to determine the value of I_0 and N_0. The ideal read out for a non-exposed pixel is 0, so it is expected that the data acquired with no radiation and varying exposure time will lay on a straight line:

$$R = N\_0 + I\_0 * t \qquad \text{[Eq.9-1]}$$

The data will be fitted thus estimating I_0 and N_0. I_0 is expected to be negligible.

This data will be used also to recognize the saturated pixels (i.e. higher than a certain threshold with no radiation input).

► *Flat field images* in order to correct for gain disuniformities and geometry projection deformation. These data will also be used to recognize the "dead" pixels (i.e. lower than a certain threshold also when significantly exposed).

A homogeneous read out is expected on the whole detector, except for the noise read out already estimated from the dark field data in the previous calibration step. Flat field images will be acquired with different radiation exposures and photon fluencies in order to better estimate the value of G and check the independence of the gain correction from the impinging photon rate.

A normalization factor will thus be calculated in order to correct for the disuniformities.

Gain disuniformities will be related to the detector element, while geometry deformations will be related to its position.

The more the data acquired both for dark and flat field, the better the pre-processing fixed pattern correction will perform.

9.2 Controller modules

9.2.1 Calibrating the “simplistic” steering algorithm

We have implemented a dedicated algorithm for calculating the thresholds used by the steering algorithm to switch between exposures for the second scan.

The algorithm is based on first capturing images of a dedicated test object with all possible exposure available (0-100% filter setting). Each image should have consistent exposure for the entire image, and the test object must not be moved between exposures. The test object should be a sloped object, where density increases from 0 up to a level somewhat exceeding the maximum expected density of any "real" object. The exposure settings must be chosen beforehand, and the exposure range should fit any real objects that will be imaged.

The algorithm establishes the thresholds by comparing regional 95 percentile responses in the scout scan with corresponding responses in the second scan. A linear model is fitted between the two responses, ignoring saturated pixels. The linear model is used for estimating the correct threshold. See Figure 6-14 for an illustration of the algorithm.

A dedicated Matlab routine – calculateSteeringThresholds – is then used to calculate the thresholds used by the steering algorithm. In addition to the actual images taken during these test exposures, the routine needs the threshold value that should be employed for steering. As previously mentioned, this threshold needs to be established empirically.

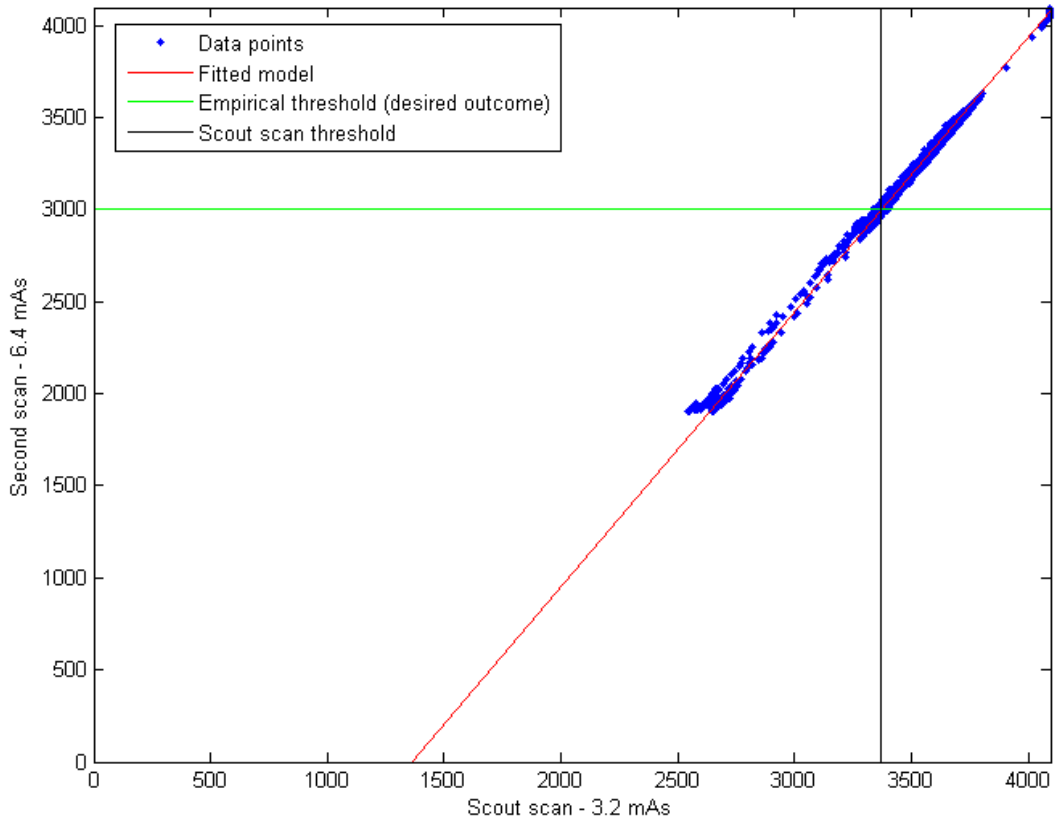

Figure 6-14: Example output and algorithm illustration of threshold selection algorithm. Blue points indicate 95 percentile responses for corresponding regions in scout scan and second scan. Green line indicates desired threshold for final exposure (empirically established). Black line indicates threshold for when this exposure becomes insufficient – if the scout scan regional values are above this threshold, more exposure is necessary. If not, this or a lower exposure is sufficient.

The routine will output a set of thresholds according to the calibrating images which can be used directly in the steering algorithm.

Please note that these thresholds will be sensitive to changes to the sensor, so for instance changing gain settings or similar will require a different set of thresholds to be used.

9.3 Post-processing modules

9.3.1 Noise pre-filtering

A first stage within the post-processing loop can be a preliminary noise reduction filter, in order to avoid excessive design specifications for the main image restoration stage. The noise pre-filtering module can realize spatial low-pass convolution masks in order to remove artifacts smaller than a specific size, which is defined by *the smallest exploitable clinical feature*. For a spatial resolution of 32x32 um, a lower limit on the size of microcalcifications equal to 0,3 mm corresponds to 10-pixel objects. Thus, a preliminary noise reduction can safely remove speckle or other type of noise with spatial size less than 10 pixels, *without destroying the clinical value of the image*.

Additionally, case-specific noise filters can be incorporated when specific inefficiencies of the acquisition system can be accurately modeled. For “bad” pixels introducing white and black single-pixel speckling, a “Salt & Pepper” de-noising filter can be used to correct the input image data before any other processing takes place (see Table 8-1 in section 8.1.1).

9.3.2 Image restoration filter

The main post-processing stage is constituted by the sophisticated image restoration filter, probably realized as a non-zero mean spatially varying Wiener filter, as described in section 8.1.2. The design and implementation of such a filtering module requires detailed measurements of the spatially-varying PSF function, as well as the noise characteristics of the system. Thus, a custom set of test data are needed as guidelines and base for measuring the statistical properties of the complete acquisition process.

As described in section 8.1.1, the image observation model includes distortion effects that are usually the result of detector inefficiencies, electronic interference, as well as beam scattering in the system and the target object itself. In order to quantify and measure the combination of these distortions accurately, a set of *test pattern phantoms* of well-described mathematical and physical properties are presented to the system. The cumulative degradation effects are estimated by measuring the resulting image, i.e. amount of distortion introduced by the acquisition system itself. Thus, the quality and nature of these test pattern phantoms are extremely important for the efficiency of the resulting image restoration model.

In I-ImaS, there are three dominant degradation factors that contribute to the distortion effects:

- non-uniform *sensor IC movement* in micron level
- non-uniform X-ray beam geometry due to *varying deflection angle*
- possibly non-uniform *noise* distribution over the entire scanning area

If one or more of the above statements is true for the final I-ImaS system, the resulting PSF will not be constant, thus the acquired images will be spatially non-stationary in terms of distortion. In order to address these problems, the test

pattern phantom has to be designed in a way that reveals these inconsistencies at the highest possible degree.

Non-uniformities in the X-ray beam geometry results in geometric distortions of the pixels that are produced on the projection (flat) plane. This type of effects can be modeled mathematically, if the exact geometry of the X-ray (point) source against the projection (flat) plane is known, or they can be calculated directly in terms of spatially-varying PSF function. Figure 9-1 illustrates the visual effect of this type of distortion in magnification.

(a) Original image (b) Geometrically distorted image

Figure 9-1: Non-uniformities in the X-ray beam deflection when using point X-ray source and flat projection plane.

The line-scanning procedure introduces a relative movement of the detector in the sensor IC movement and the exposed tissue area. This results in a motion "blurring effect" in micron level that can be very significant when the integration time of the sensor IC becomes relatively comparable with the scanning speed. It should be noted that the "step-and-shoot" line-scanning method limits these motion effects significantly, however instant stopping and starting motor steering is mechanically impossible. Furthermore, the scanning speed and accuracy can not be controlled in a perfect manner along the entire scanning axis. In this case, the detector movement is non-uniform and the resulting distortion is also spatially-varying. Figure 9-2 illustrates the visual effect of "motion blurring" distortion for various scanning speeds.

(a) Original image (b) Horizontally motion-blurred image

Figure 9-2: Motion blurring effects from relative movement between the object and the detector during image scanning.

These two types of distortion effects can be measured accurately using a test pattern that illustrates the spatially-varying PSF function throughout the entire projection plane. Since the width of the PSF is directly related to the restoration (Wiener) filter size, a simple approach is to design a test pattern of well-defined grid with points of minimal size. Such a grid can be similar to the ones presented in Figures 9-1 and 9-2, only in much smaller scale, typically a small multiplicand of the system's theoretical spatial resolution, i.e. N pixels in size or Nx(32x32) um in physical width. For a typical PSF with width smaller than 16x16 pixels, the test grid should contain measuring "peaks" with 8-pixel width at most, i.e. 0,256 mm in physical dimensions. Figure 9-3 illustrates such a test pattern grid in its initial form (a) and in its degraded form (b) when measured through the acquisition system.

(a) Original image (b) Spatially-varying PSF image

Figure 9-3: Suggestive prototype test pattern grid for measuring spatially-varying PSF. Sample (a) is the original grid and (b) is the expected resulting image when measured through the acquisition system.

According to the results obtained by the analysis of the DB3 mammographic image database, the noise level rises in a near-linear logarithmic rate as mAs setting increases, while increase in kVp results in larger slope values [A03]. As already mentioned in section 5, the current design of the first I-ImaS prototype specifies the kVp setting as an "external" fixed system parameter that will be set by the operator prior to the line-scanning procedure. On the other hand, changes in the mAs setting will be effectively simulated using a set of sliding wedge filters with step-wise absorption factors. Although the general form of the overall noise of the prototype X-ray source has been measured and modeled, it is not certain if these assumptions will hold true for the final prototype I-ImaS system. Furthermore, it is not certain if these noise measurements contain multiplicative, as well as additive, noise factors, as the mAs setting is actually simulated by different absorption factors.

In order to assess the true nature and power spectrum of the noise for all (simulated) mAs values, a complete scan of the background for each constant mAs setting has to be registered for noise modeling, as well as the estimation of the true dynamic grayscale range in each case. This procedure can be easily realized by successive scans with increasing mAs setting for every new scan, since no test pattern phantom and no filter estimation is required. The use of step-wise sliding wedge filters limits mAs to a set of discrete values (typically 5-6 settings) and the external kVp "mode" selector also limits its values to a small discrete set (typically 3 settings). Therefore, even in the case of complete spatially-variant realization of noise modeling, only a limited set of successive scans are required (i.e. 5x3 = 15

complete scans). Since the noise is generally considered to be independent of the projected object (intra-tissue beam scattering is considered negligible in relation to other dominant noise factors), the noise modeling procedure can be conducted separately from the PSF and Wiener filter calculations described previously.

The models used for implementing the controller itself require some partial initialization by the current dynamic grayscale range. This is due to the fact that inverse modeling, applied for feedback calculation, includes various textural feature values that are directly or indirectly related to the current grayscale. For example, the "simplistic" steering model, presented in detail in section 6.3, requires an accurate estimation of the "foreground" object against the "background" plane as a quality characteristic. Therefore, the true grayscale range has to be calculated over specific homogeneous areas of the image, namely over pure "black" (saturated) and pure "white" (non-exposed) regions.

Both grayscale histogram and noise model can be estimated by a series of successive scans over the entire projection plane, each time using a pair of fixed kVp ("mode") and fixed mAs (wedge filter position) settings. The resulting set of template images can be used as guidelines for noise power spectrum and dynamic grayscale range estimations, even in spatially-variant cases. Figure 9-4 demonstrates the resulting grayscale saturation and different noise effects when using different kVp and mAs settings.

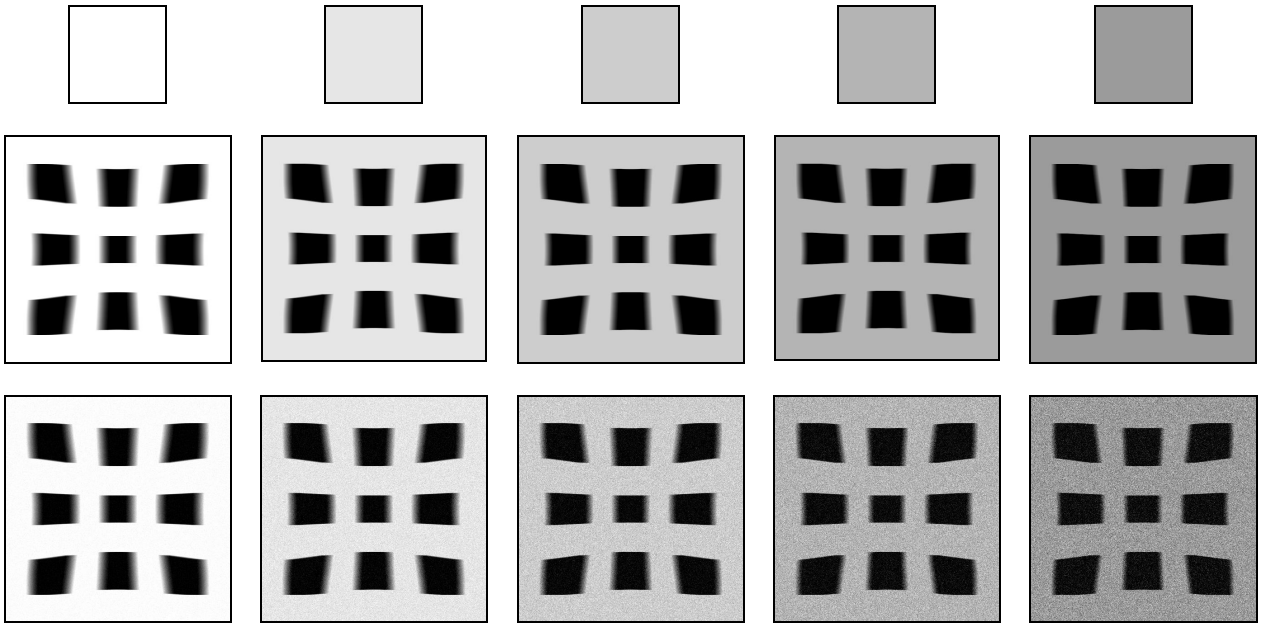

Figure 9-4: Demonstration of different noise effects when using different kVp and mAs settings in successive scans.

If the I-ImaS prototype system is proved not to be spatially stationary or if it is difficult to prove otherwise, a full spatially-variant realization version of the complete image restoration stage must be implemented. In this case, the exact (x,y) position of the current image sample, as well as the exposure settings (kVp,mAs), can be used as a compound index for a filter bank of spatially-variant restoration model realizations. This essentially means that for each location on the

projection plane and for the current exposure parameters, a different set of restoration & noise model can be used in the form of a pre-calculated Wiener filter. Since the complete image restoration stage will be implemented as a separate software module that processes the image data off-line, the computational complexity and storage requirements of such a realization is not a significant issue. Such a filtering mechanism, incorporating non-stationary properties regarding both the spatial location and the exposure parameters, can prove highly efficient and adaptive to any type of inefficiencies of the prototype I-ImaS system.

The off-line calibration procedure described previously can be summarized in the following steps:

1. One-time scanning of a uniform test pattern phantom (grid) over the entire projection plane, in order to estimate the spatially-variant PSF.
2. Successive scans over the entire projection plane, each time using a pair of fixed kVp ("mode") and fixed mAs (wedge filter position) settings, for estimating noise and grayscale range in each case.
3. Combine the results of step 1 and 2 to implement filter banks of variant Wiener restoration filters.

An additional, more restricted, version of the calibration procedure can also be embedded within the line-scanning procedure. The incorporation of special homogeneous "black" (saturated) and "white" (non-exposed) areas within each normal image, as well as specific wedge filter positioning at the beginning of the scan, can provide valuable information about the current performance of the system and its conformance with the expected operational profile. Essentially, while the Wiener filters used for completed image restoration are too complex to calculate on every run, the grayscale and noise parameters can be easily estimated by using a few simple "testing areas" embedded within each scanned image data. Figure 9-5 demonstrates how the projection plane can be properly adjusted in order to embed these types of testing areas automatically in every scan.

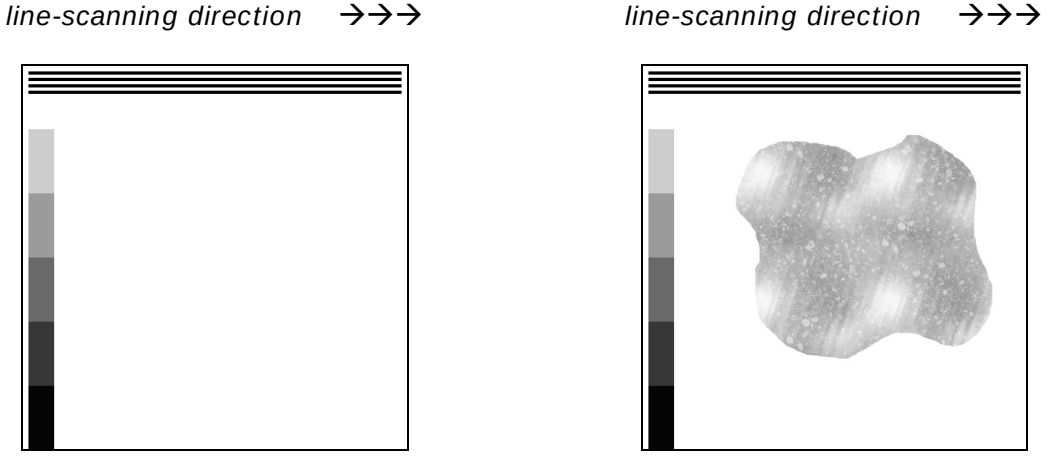

(a) Empty projection plane template

(b) Sample image with embedded patterns

Figure 9-5: Suggestive template for embedded test patterns within the projection plane.

Suggestive References:

[A01] S.Theodoridis, D.Cavouras, H.Georgiou, "I-ImaS: Preliminary Analysis Report and Proposed Design", Dept. of Informatics & Telecomm., Univ. of Athens, Greece, Mar.2004.

[A02] C.J.Martin, D.G.Sutton, P.F.Sharp, "Balancing patient dose and image quality", Applied Radiation and Isotopes, 50 (1999) pp.1-19.

[A03] I-ImaS, Workpackage 3 – Deliverable D.8, "Translating information signatures to a sequence of well-defined processing functions", Dec.2004.

[A04] A.K.Jain, "Fundamentals of Digital Image Processing", Prentice-Hall: 1989.

[A05] J.V.D.Vegte, "Feedback Control Systems", Prentice-Hall: 1994.

[A06] S.Haykin, "Adaptive Filter Theory", 3rd/Ed., Prentice-Hall: 1996.

[B01] R.M.Haralick, K.Shanmugam, I.Dinstein, "Textural features for image classification", IEEE Trans.Sys.Man.Cyb., Vol.SMC-3, No.3, Nov.1973, 610-621.

[B02] R.M.Haralick, "Statistical and structural approaches to texture", Proc.IEEE, Vol.67, No5, May 1979, 786-804.

[B03] M.Galloway, Texture analysis using gray level run lengths, Comp.Graph.Im.Proc., 4, 1975, 172-179.

[B04] Gonzalez, R.C.; Woods, R.E. Digital Image Processing. USA: Addison-Wesley, 1992.

[C01] R.E.Kalman, "A New Approach to Linear Filtering and Prediction Problems", Trans.ASME Ser.D., J. Basic Engineering, 82 (1960): 35-45.

[C02] W.T.Miller, R.S.Sutton, P.J.Werbos, "Neural Networks for Control", MIT Press: 1990.

[C03] M.Jamshidi, N.Vadiee, T.J.Ross, "Fuzzy Logic and Control", Prentice-Hall: 1994.

[D01] S.E.Umbaugh, "Computer Vision and Image Processing", Prentice-Hall: 1998.

[D08] A.K.Jain, S.Ranganath, "Applications of two-dimensional spectral estimation in image restoration", Proc.ICASSP-1981 (May 1981): 1113-1116.

[D18] S.Twomey, “On the numerical solution of Fredholm integral equations of first kind by the inversion of linear system produced by quadrature”, J. Assoc. Comput. Mach. 10 (Ja. 1963): 97-101.

[D19] B.R.Hunt, “The application of constrained least squares estimation to image restoration by digital computer”, IEEE Trans. Comput. C-22 (Sept. 1973): 805-812.

[D22] D.G.Luenberger, “Introduction to Linear and Nonlinear Programming”, Reading, Mass.: Addison-Wesley: 1973.

[D23] T.S.Huang, D.A.Barker, S.P.Berger, “Iterative Image Restoration”, Applied Optics 14, No.5, (May 1975): 1165-1168.

[D24] E.S.Angel, A.K.Jain, “Restoration of images degraded by spatially varying point spread functions by a conjugate gradient method”, Applied Optics 17 (July 1978): 2186-2190.

[D30] N.E.Nahi, “Role of recursive estimation in statistical image enhancement”, Proc. IEEE 60 (July 1972): 872-877.

[D31] A.O.Aboutalib, L.M.Silverman, “Restoration of motion degraded images”, IEEE Trans. Cir. Sys. CAS-22 (Mar. 1975): 278-286.

[H01] Huda W, S. A., Ogden KM, Dance DR. (2003). "Experimental investigation of the dose and image quality characteristics of a digital mammography imaging system." Med Phys. 30(3): 442-8.